The Pennsylvania State University

The Graduate School

LIPID BIOMARKER RECORDS OF ENVIRONMENTAL CONDITIONS AND HABITATION DURING THE MID-NEOLITHIC (DALMATIA COAST, CROATIA)

A Thesis in

Geosciences

by

Emma Hartke

Submitted in Partial Fulfillment
of the Requirements
for the Degree of

Master of Science

August 2022

The thesis of Emma Hartke was reviewed and approved by the following:

Katherine H. Freeman
Evan Pugh University Professor
Professor of Geosciences
Thesis Advisor

Sarah J. Ivory
Assistant Professor of Geosciences

Max K. Lloyd
Assistant Research Professor of Geosciences

Mark E. Patzkowsky
Professor of Geosciences
Associate Head for Graduate Programs and Research Professor

ABSTRACT

Records of environmental change during the mid-Neolithic/Early Holocene show both pronounced global deglaciation climate trends and significant impacts from human activity. Included among these was the encroachment of human groups into Europe as they shifted from nomadic, pastoral lifestyles to more stationary, agro-pastoral lifestyles. The relationship between anthropogenic impacts and both on-going postglacial changes and punctuated climate events, however, is less clear. Separation of climate and anthropogenic signals in the paleorecord to resolve questions of timing is aided by a continuous sedimentary record that can be evaluated with a suite of geochemical tools. This study uses new abundance and distribution patterns of lipid biomarkers, including *n*-alkanes (plant wax compounds) and polycyclic aromatic hydrocarbons (PAHS; fire indicator compounds), and previously collected data including bulk organic carbon and bulk carbonate carbon and oxygen isotope records, charcoal data, pollen records, and archaeological findings to reconstruct the presence and pace of human and environmental changes during this period. These were applied to a continuous sediment core sampled from a paleolake near a mid-Neolithic human habitation site Krivače, located along the Dalmatia Coast (Croatia). *N*-alkane and PAH concentrations increased dramatically between 8000 and 6000 yrs BP, possibly due to changing climate, human activity, or a combination of both. High proportions of atypical short even-chain *n*-alkanes detected across this same interval were potentially sourced from autochthonous lake bacteria or derived from soil inputs. While PAHs increased in abundance during this interval, plant biomarker-normalized patterns did not increase, which suggests fire activity did not increase out of proportion to increased fuel loads. These patterns possibly indicate increased input of soil-derived contributions.

Results from this project inform the timing and appearance of human-environmental events. Specifically, biomarker distributions of plant-derived *n*-alkanes tracked climate trends

(temperature and hydroclimate), suggesting biomass increased with regionally under wetter conditions and decreased under drier conditions. PAH abundances, which tracked plant wax n-alkane inputs, indicated no large change in flammability was associated with habitation. The anomalous distributions between 8000 and 6000 yrs BP suggest significant inputs from human activity by soil disturbance, but also coincide with hydroclimate extremes (wetter conditions marked by flooding events) which could have also enhanced mobilization of soil-derived materials from the lake catchment. Further geochemical tools, such as fecal sterols and compound-specific isotope data, can help resolve these. The results of this study suggest human habitation during this period may have started earlier and extended beyond the timeframe currently documented by archaeological evidence. Additional studies can help us improve the timeline of early human history and reckon with human-environmental changes in a rapidly warming climate.

TABLE OF CONTENTS

LIST OF FIGURES

LIST OF TABLES

ACKNOWLEDGEMENTS

My sincerest thanks to my advisor, Dr. Kate Freeman, for her tireless guidance and support on this master's project. She provided constant encouragement, wisdom, and feedback on a project and topic on which I had no prior knowledge. Kate is a wonderful advisor, and I am so happy to have had her on my team for this project, which I would not have completed without her efforts nor become the student and scientist I am today.

I would also like to thank other members of the Freeman Lab, including Heike Betz and Allie Baczynski, for their willingness to help and their phenomenal lab expertise. I deeply appreciate their efforts to help field my questions, troubleshoot instrument errors, and everything in-between.

Thanks to my committee members, Sarah Ivory and Max Lloyd, for their time and assistance in guiding this project over the last two years. Their difficult questions and individual expertise's helped strengthen my skills as a scientist and writer.

Thanks to my collaborators, Sarah McClure, Douglas Kennett, Nikolina Ilijanić, and the previous Penn State students who have helped me with or contributed to this project, including Troy Ferland, Allison Karp, Catherine Gagnon, and Matt Wileyto. The wealth of information this team gathered over previous years was essential to interpreting my project results and building my thesis, and I am extremely grateful for their efforts.

I thank my dog, Rowan, for being my literal and metaphorical support since my sophomore year of college. I greatly appreciate our one-sided academic dialogue, friendly gossip, and late-night conversations. Even on my most challenging days, she reminds me that life is pretty good.

Finally, I thank those closest to me. To my parents who have supported my academic endeavors over the last many years and have never doubted my abilities—thank you. It is because

of your love and encouragement that I was able to pursue the field of my dreams. To my partner, Matt, who has diligently put up with me saying “after this deadline, I’ll finally be able to relax” every week for the last 2 years. Thank you for being there for me from the start of my graduate journey, I truly could not have done it without you.

1. Introduction

The current Holocene Epoch has seen some of the most rapid landscape and climate change in Earth's history. Today, these changes are primarily due to human influence, particularly increased greenhouse gas emissions since the early 1800s. But humans were modifying landscapes long before the Industrial Revolution. The Holocene Epoch (11.7 kyr–present) overlaps with the start of the Neolithic (9–6.9 ka). During the Neolithic Revolution, humans transitioned from nomadic hunter and gatherer lifestyles to more settled, agro-pastoralist lifestyles. This is regarded as one of the most important transitional events in human history and the entryway to modern civilization (Weisdorf, 2005; McClure & Podrug, 2016). The Dalmatia Coast, the Croatian coastline bordering the eastern Adriatic Sea, is an excellent location to study this transitional window. Not only was this the most populous region of Croatia during the Neolithic, but its coastal valley soils were some of the most fertile in the area (McClure & Podrug, 2016). Together, these conditions make an ideal case study to observe how a relatively untouched landscape changed as a result of intensifying human activity by early farming practices.

Alongside human activity, the Adriatic landscape was also changing with climate. The beginning of the Holocene marked the end of the last glacial period (11.7 kyr) and the transition to a deglaciation (warming) period. This region is strongly affected by temperature and hydroclimate changes, as its geographic position is at the confluence of several major atmospheric systems. Additionally, variations in climate and solar activity triggered the onset of multiple, semi-cyclical periods of extensive ice-rafting into the North Atlantic, called Bond events. These events took place approximately every 1500 years and were tied to major swings in hydroclimate in the Mediterranean, including the Adriatic region (Bond *et al.,* 1997; Bond *et al.,*

2001; Zielhofer *et al.,* 2008). General climate trends in the Adriatic evolved from cool and humid conditions during the Early and Middle Holocene towards warm and arid conditions from the Middle to Late Holocene (Jalut et *al*., 2009).

Climate change is often cited as the key driver of landscape change during the Holocene and as a control on human movement and settlement, including in the eastern Mediterranean (Jalut *et al*., 2009). Case studies from multiple continents show that periods of severe precipitation or drought conditions, for example, likely caused human groups to adapt or abandon their settlements (Hodell *et al.,* 1995; Weiss & Bradley, 2001; Simonneau *et al.,* 2013; Giguet-Covex *et al*., 2013). In the eastern Mediterranean, human groups increased land-use activities and implemented new technologies during wet (or less arid) climate conditions (Weiss & Bradley, 2001). At the same time, human activity likely amplified ecological responses to regional climate changes. For example, pollen evidence from sites in the central Mediterranean suggest there was a higher proportion of resilient scrubland vegetation during the Middle and Late Holocene, coinciding with climate-driven aridification. Higher proportions of scrublands over deciduous woodlands were encouraged by biomass burning, grazing, and crop cultivation that eliminated less tolerant vegetation types (Di Rita & Magri, 2012).

In this study, we posit that shifting climate patterns were mainly responsible for landscape changes in the sensitive eastern Mediterranean region during the Holocene. Here, we consider *landscape changes* to include conditions related to vegetation character and composition across a given area, along with potentially related changes in soil composition, transport processes, relief, and water levels. We suggest that changes and trends in geochemical and biological markers will primarily reflect responses to climatic perturbations rather than human activity, and that signs of human land-use will be minimal or overprinted by these other large-scale events. We believe the strong gradients in climate and conflicting atmospheric systems in this region produced much stronger changes to the landscape than emerging human agricultural

activity in its beginning stages. Additionally, archaeological records provide multiple case studies demonstrating repeated events of societal collapse following major climatic events, suggesting that climate is the main driver of vegetation, soil, and other landscape changess, and an important control on human activity (Hodell *et al.*, 1995; Weiss & Bradley, 2001; Simonneau *et al.*, 2013; Giguet-Covex *et al*., 2013). Determining the magnitude and pace at which changing climate and human activity altered landscapes in the Dalmatia Coast, and whether these were independent or compounding processes, is aided by the use of geochemical proxies. Geochemical records are advantageous because they act as indicators of environmental change, and have the ability to reconstruct major trends in environmental parameters such as temperature, hydroclimate, vegetation, weathering, and primary productivity.

Lipid biomarkers are natural compounds derived from plants, animals, algae, or microbes in the environment. They are ubiquitous, readily obtained from lake sediment cores, and relatively resistant to degradation. The types and distributions of different biomarker compounds reflect changes in sources and environmental processes. We specifically evaluated vegetation change and associated shifts in terrestrial carbon inputs to lake sediments, and evidence for changing fire frequency using *n*-alkanes derived from leaf waxes and polycyclic aromatic hydrocarbons (PAH) derived from biomass burning. If climate was the dominant control on landscape changes, then we expect that overall abundances of *n*-alkanes increased during cool, wet climatic periods and decreased during hot, dry climatic periods in patterns that reflected shifting abundances and communities of terrestrial vegetation. Additionally, we expect that abundances of PAHs will covary with trends in biomass (indicated by *n*-alkanes) based on an assumption that covarying fire signatures reflect biomass fuel stocks. If they did not covary, this would suggest an increase in fire occurrence due to biomass burning associated with settlements and early farming practices.

1.1 *N*-alkanes

N-alkanes are simple hydrocarbons that form the waxy epicuticular coating of vascular plant leaves. They typically have odd chain lengths and their abundance and distribution patterns in a suite of samples reflect inputs from local vegetation (Eglinton, 1962; Eglinton & Hamilton, 1967; Freeman & Pancost, 2014; Diefendorf & Freimuth, 2017).

1.1.1 Chain length

Chain lengths for terrestrial plant waxes range from approximately 27 to 35 carbons (C_{27} to C_{35}; some plants synthesize similar aliphatic compounds with even longer chain lengths; Eglinton & Hamilton, 1967). The 27–35 lengths in the homologous series are typically the most abundant and considered indicative of terrestrial plant inputs (Freeman & Pancost, 2014; Yu *et al.*, 2016; Diefendorf & Freimuth, 2017). Even so, the chain lengths C_{27} to C_{31} have mixed sources of terrestrial origin (Freeman & Pancost, 2014; Diefendorf & Freimuth, 2017). In the eastern Mediterranean and Adriatic, these chain lengths are typically derived from deciduous vegetation but may also be produced by herbs, trees and shrubs (Norström *et al.*, 2017). Chain lengths C_{33} to C_{35} have been attributed to grassy plants and C4 vegetation in African floras, but in the Mediterranean, where C4 plants are not dominant, herbs, trees and shrubs are the main contributors of these chain lengths (Freeman & Pancost, 2014; Norström *et al.*, 2017; Diefendorf & Freimuth, 2017). Plant wax abundances are sensitive to the proportion of angiosperm and gymnosperm inputs, as angiosperms have been shown to produce higher quantities of longer chain lengths ($>C_{27}$) compared to gymnosperms ($<C_{27}$; Liu *et al.*, 2018).

Short ($<C_{21}$) and mid-chain *n*-alkanes (C_{21} to C_{25}) have less clear environmental sources. Authors attribute these chain lengths to inputs from lower and intermediate vegetation types,

including algae, lichens, Sphagnum, and aquatic macrophytes or a combination of these (Ficken *et al.*, 2000; Freeman & Pancost, 2014; Yu *et al*., 2016; Diefendorf & Freimuth, 2017).

1.1.2 Odd and even-chain preference patterns

It is common for plant-derived *n*-alkane distributions to demonstrate an odd-over-even preference pattern for chain lengths. Odd chain lengths are produced when even-numbered alkyl acids, biosynthesized from acetyl CoA, are elongated and decarboxylated (Eglinton *et al*., 1967; Jetter & Kunst, 2008; Freeman & Pancost, 2014; Diefendorf & Freimuth, 2017). *N*-alkane distributions with an even-over-odd preference pattern (discussed below) are unusual and attributed to diagenetic processes, extreme (hypersaline or anoxic) environmental catchment conditions, or bacterial or algal inputs (Kuhn *et al*., 2010; Wang *et al*., 2010).

1.1.3 Even-numbered short-chain *n*-alkanes

N-alkane distributions are normally dominated by odd, long-chain homologues. *N*-alkane distributions dominated by even, short-chain homologues are uncommon and traditionally attributed to lower and sub-vascular plant inputs and the processes described above for the production of even-over-odd distributions (Kuhn *et al.*, 2010). However, recent studies suggest that even, short-chain *n*-alkane distributions are more common than previously described. They appear to be sourced by direct formation in vascular plants, microbes, or potentially formed via microbial or thermal alteration of odd *n*-alkanes in soils, or in petroleum or other fossil fuels.

Kuhn *et al.* (2010) found woody plants and grasses can directly produce even-numbered short-chain *n*-alkanes (i.e., C_{14}–C_{20}) in their plant tissues, and that similar distributions also occur in some woodland and grassland soils in arid environments (Kuhn *et al.* 2010). Their study also

showed, for both primary plant tissues and soils, two *n*-alkane groups were present: even, short-chain homologs and odd, long-chain homologs. In the studied plant tissues, the odd, long-chain homologues were dominant relative to the even, short-chain compounds. Notably, the opposite was true in the corresponding soils, wherein even, short-chain alkanes were more abundant than the odd, long-chain alkane homologues (Kuhn *et al.* 2010). The authors suggested the observed even-over-odd preference patterns could be due to microbes that colonized plant tissues or soil fungi in humid environments (Jansen *et al.* 2008). Kuhn *et al.* (2010) argued an even-over-odd preference patterns derived directly from local vegetation and soils, and not from aquatic microbial sources.

Upward seepage of ancient hydrocarbons from deep source rocks can produce even-numbered short-chain *n*-alkane distributions in soils or lake sediments (C_{16}–C_{18}; Palacas *et al.*, 1972; Lichtfouse *et al*., 1997; Fiket *et al*., 2008; Kuhn *et al.*, 2010). This occurs when petroleum-based hydrocarbons from ancient sediments or deep source rocks migrate upward through porous rock and mix with existing *n*-alkanes deposited in sediments, significantly altering the resulting *n*-alkane distribution from the primary signature of biological sources. This phenomenon has been observed in karst-dominated landscapes (Lichtfouse *et al*., 1997). It should be noted, however, that *n*-alkane distributions sampled directly from crude oil are thermally mature and therefore do not usually have strong odd-over-even (or even-over-odd) chain length preferences for C_{17}–C_{29} alkanes (Farrington & Meyer, 1975; Nishimura & Baker, 1986). The presence of a chain length preference potentially indicates that additional degradation processes occurred at some point between oil formation and upward seepage, likely associated with microbial activity (Escobar *et al.*, 2011).

Alternatively, several studies have demonstrated that biomass burning can produce high amounts of even, short-chain *n*-alkanes (C_{16}–C_{18}) in soil organic matter, suggesting these compounds might serve as an additional proxy for fire activity (Dettweiler *et al*., 2003;

Weisenberg *et al*., 2009; Eckmeier *et al.*, 2009; Kuhn *et al.*, 2010). Experiments show that soils heated to natural wildfire and controlled-burn temperatures (360°C) and biomass charred at even higher temperatures (400–500°C) have distinct *n*-alkane distributions before and after burning, with typical odd, long-chain *n*-alkane distributions prior to burning (dominated by odd homologues from C_{27} to C_{31}) and even, short-chain *n*-alkane distributions after burning (dominated by even homologues from C_{16} to C_{20}). The different patterns are seemingly due to thermal transformations that break down odd, long-chain *n*-alkanes (e.g., thermal degradation; Dettweiler *et al*., 2003; Weisenberg *et al.*, 2009).

Wang *et al*., (2010) suggest that even, short-chain homologues (C_{16}–C_{20}) may also be produced by autochthonous bacteria from odd, long-chain homologues after deposition in anoxic or weak-oxic lacustrine settings, especially in arid environments (Wang *et al.*, 2010). Some bacteria produce even, short-chain *n*-alkane distributions between C_{12} to C_{22} with maxima at one or two carbons, consistent with the characteristic bimodal distribution of an *n*-alkane profile (Elias *et al.*, 1977; Ekpo *et al.*, 2005). The mechanism underlying bacterial production of these *n*-alkanes is unclear, but potentially occurs via post-depositional alteration of algal material, including reduction of fatty acid or other even lipid compounds, by direct contributions from microbes, or from a combination of these processes (Nishimura & Baker, 1986; Ekpo *et al.*, 2005; Wang *et al.*, 2010). Wang *et al.* (2010) argued for bacterial production as the source for a predominant grouping of even, short-chain *n*-alkanes in lacustrine sediments alongside a secondary less-abundant grouping of odd, long-chain *n*-alkanes from normal terrestrial sources (Wang *et al*., 2010). Similarly, previous studies (Palacas *et al.*, 1972; Simoneit, 1977a; Nishimura & Baker, 1986; Ekpo *et al.*, 2005) that reported even short-chain *n*-alkane distributions also suggested they potentially were produced by bacterial sources in other marine, coastal, and freshwater settings.

Wang *et al.* (2010) were the first to tie even alkanes to bacterial inputs for a continuous lacustrine sedimentary section, which the authors considered to be natural to the environment (i.e., autochthonous bacteria). However, they did not identify specific taxonomic information or metabolic properties of the microbes. This is likely because the pool of possible bacterial sources is exceedingly large, and production of even, short-chain *n*-alkanes may be a result of diverse contributions from different microbial species (Ekpo *et al.*, 2005). However, findings from Cravo-Laureau *et al.* (2005) and Callaghan *et al.* (2008) demonstrate that glycyl radical-type enzymes found in sulfate-reducing bacteria and mono or dioxygenase enzymes found in sulfate-reducing, nitrate-reducing, and methanogenic microbes are capable of *n*-alkane degradation in anaerobic conditions (Cravo-Laureau *et al*., 2005; Callaghan *et al.*, 2008). *N*-alkane degradation using these enzymes occurs differently depending on the strain of microbe, and degradation pathways can vary significantly (Cravo-Laureau *et al*., 2005).

1.2 PAHs

Polycyclic aromatic hydrocarbons, or PAHs, are multi-ring aromatic hydrocarbons formed during the incomplete combustion of organic material (Blumer & Youngblood, 1975; Denis *et al*., 2012; Kappenberg *et al*., 2019; Denis *et al*., 2019; Karp *et al*., 2020). These molecules have increasingly been used as a proxy for vegetation burning and fire activity in modern and ancient sediments (Karp *et al*., 2020; Vachula *et al*., 2022). Whereas charcoal counts and tree-ring fire scars have traditionally been used as fire indicators, the depositional conditions and sampling distribution required to produce strong evidence of fire activity can complicate results and lead to ambiguous or biased interpretations (Denis *et al*., 2012; Kappenberg *et al.*, 2019; Karp *et al*., 2020). Conversely, size, abundance, and resilience of PAHs in sedimentary archives makes them valuable indicators of local fire regimes. Burned substrates influence the

relative distribution patterns of PAH compounds, allowing us to also differentiate between PAHs sourced by pyrogenic (biomass fuel) versus petrogenic (fossil carbon fuels, such as coal or oil) burn events (Denis *et al.*, 2012; Karp *et al*., 2020).

Biomass and fossil carbon-sourced PAH compounds are chemically distinguished from one another by the extent of alkylation of the aromatic rings, patterns that are likely caused by the different fuel chemical structures (Blumer & Youngblood, 1975). While some argue this occurs because differences in burn temperature directly affect the rate of transformation and therefore the composition of the final PAH structure (Blumer & Youngblood, 1975), Karp et al. (2020) did not find a strong association of temperature with PAH distributions. Biomass fires, especially involving hardwoods, typically favor unsubstituted PAH products with no alkylation (0 methyl groups, also called parent PAHs), whereas petrogenic sources tend to produce alkylated PAHs (commonly 1, 2, or 3 methyl groups). PAH distributions produced by biomass combustion processes typically have decreasing abundances of 0- to 3-methyl groups (Blumer & Youngblood, 1975; Stogianiddis & Laane, 2015; Karp *et al.*, 2020). This is corroborated by experimental burning results applying the alkylated PAH derivative index (APDI), a metric used to compare the relative proportions of parent and alkylated PAHs (methyl-, dimethyl-, and trimethyl-forms) in a sample to inform biomass fire versus fossil fuel-derived sources of PAHs in sedimentary records (Karp *et al.*, 2020).

The APDI is a metric that quantifies samples and was designed to reveal whether their source was pyrogenic or petrogenic as a screening tool. However, burns fueled by conifers can complicate APDI interpretations because they produce anomalous alkylation patterns and APDI values that appear petrogenic (Karp *et al.*, 2020). APDI values reflecting petrogenic sources should be interpreted cautiously and against the alkylated PAH retene (retene/3-ring ratio; eqn. 5) to rule out inputs from conifer burning (Karp *et al.*, 2020).

Karp et al. (2020) found that the number of aromatic rings in a PAH structure were more strongly tied to transport mechanisms than temperature. PAHs transported through soil and surface processes (ash residues) tend to contain a higher proportion of larger ring structures than those transported by smoke (Karp *et al.*, 2020). The rate and temperature of biomass burning only weakly influences the number of aromatic rings in PAHs. However, smaller PAHs are volatilized more readily than larger structures, and are more abundant in smoke (Karp *et al.*, 2020). Thus, transport mechanisms, which are sensitive to size-related physical and chemical PAH properties, influence the distributions of ring structures more so than burn rate and temperature (Karp *et al.*, 2020).

PAH structures can also be weathered directly from oil or coals. There are congener forms that reflect slow, geological maturation of organic matter and that differ from the ring structures formed rapidly during combustion processes. As a result, the congener ratios can distinguish rapid combustion inputs from slowly formed (geologically sourced) fossil compounds in the environment (Wang et al. 1999; Stogiannidis & Laane, 2014; Lyons *et al.*, 2020). Alkylated PAHs are invoked as indicators of fossil sources of PAH, whether from thermogenic or petrogenic burning processes (Blumer & Youngblood, 1975; Karp *et al*., 2020). Rapid formation via burning of either biomass or fossil carbon produces the kinetic ring configurations (alkylated naphthalenes, phenanthrenes, fluorenes, dibenzothiophenes, chrysenes, and retene) that can distinguish fire-derived inputs from oil seeps or other hydrocarbon sources (Wang *et al.*, 1999; Lyons *et al*., 2020). Parent PAHs are typically indicators for biomass fire activity, either from anthropogenic or natural (wildfire) sources. Comparing the relative proportions of parent and alkylated PAHs, while weighing possible contributions from burns fueled by conifers, can inform biomass fire versus fossil fuel-derived sources of PAHs in sedimentary records (Karp *et al.*, 2020).

1.2.1 Parent PAHs

Parent PAHs are aromatic hydrocarbon rings without any branching or alkyl substitutions. Key diagnostic parent PAHs derived from biomass burning have been identified and reported by previous authors (Denis *et al*., 2012; Karp *et al.*, 2020), and their pyrogenic origins are typically confirmed using additional PAH ratios and indices (e.g., alkylated PAH derivative index, pyrene/3-ring ratio; Karp *et al*., 2020; Lyons *et al*., 2020). Here we focus on the relative abundances of three parent PAHs (phenanthrene, fluoranthene, and pyrene) that are most strongly associated with biomass burning (Stogiannidis & Laane, 2015; Karp *et al*., 2020) for their utility as a primary fire proxy.

1.2.2 Alkylated PAHs

Alkylated PAHs are distinguished from parent PAHs by methyl or short linear or branched alkyl substitutions on the aromatic ring structure (Denis *et al.*, 2012). Alkylated PAHs with multiple methyl groups are typically sourced from petroleum or other fossil carbon sources (Blumer & Youngblood, 1975; Denis *et al.*, 2012; Stogiannidis & Laane, 2015; Lyons *et al*., 2020). However, similar structures are also produced by burning of conifer biomass, likely due to the presence of terpenoid compounds associated with resins (Karp *et al.*, 2020). Alkylated PAHs are numerous, although methylated homologs of phenanthrene (methylphenanthrene, dimethylphenanthrene, and trimethylphenanthrene) are of the most widely reported and used in different metrics and indices (Karp *et al*., 2020). Here, alkylated PAHs (retene and methylated homologs of phenanthrene) were examined alongside parent PAHs to examine changes in potential fuel sources (Stogiannidis & Laane, 2015; Karp *et al*., 2020).

Where fossil carbon sources are absent, alkylated PAHs can also be produced by microbial alteration, potentially associated with organic weathering within soils (Johnsen *et al.*, 2005; Karp *et al.*, 2021). Alkylation hinders microbial decomposition of the ringed structures by hindering degrading enzymes and decreasing PAH solubility in water (Johnsen *et al.*, 2005; Zhang *et al.*, 2006; Karp *et al.*, 2021). As a result, weathering and related degradation processes cause overall loss but result in relatively enhanced abundances of alkylated over parent PAHs (Johnsen *et al.*, 2005; Zhang *et al.*, 2006; Karp *et al.*, 2021). A weathered soil profile could therefore account for elevated APDI values and elevated alkylated PAH patterns, as suggested by Karp *et al.* (2021).

2. Background

2.1 Regional setting

The Dalmatia Coast is an expansive coastal region of Croatia that extends approximately 350 km northwest to southeast and borders the Adriatic Sea, the northernmost arm of the Mediterranean. The regional geology of Dalmatian Coast is characterized by a large Cretaceous–Paleogene (125–25 Ma) carbonate karst platform overlying Precambrian bedrock and other thin sedimentary units (Lončar *et al.*, 2017). The carbonate platform extends laterally and forms most of the Adriatic Basin (Podrug *et al.*, *in press*).

The Bribir-Ostrovica valley, located on the southeastern edge of the Dalmatia Coast, is one of Croatia's many carbonate valleys and rich with fertile soils and freshwater sources (McClure, *under review*). The valley is flanked by Quaternary alluvium and hosts Quaternary lake sediments near its center (Podrug *et al.*, *in press*).

2.2 Regional climate

Climate along the Adriatic Coast today is generally temperate, characterized by dry, warm summers and humid, mild winters (Köppen, 1932; Combourieu-Nebout *et al.*, 2013; López-Avilés *et al.*, 2021). Mean annual air temperatures along the Dalmatia Coast are approximately between 14–16°C and mean annual rainfall varies between approximately 730–1240 mm (Gajic-Capka & Zaninovic, 2006). Contemporary precipitation and river discharge are higher in the winter months and lower in summer months (Benito *et al*., 2015b; López-Avilés *et al*., 2021).

Due to its central location in the Mediterranean, which is influenced by conflicting sub-tropical and mid-latitude atmospheric patterns, climate in the Adriatic basin is dynamic and highly sensitive to regional conditions and global climate oscillations (Combourieu-Nebout *et al*., 2013; Di Rita & Magri, 2012; Benito *et al.*, 2015b). Evidence from pollen and isotope records shows that climate has fluctuated between humid to sub-humid and arid to sub-arid conditions (Jalut *et al.,* 2009). Further, global atmospheric and oceanic circulation patterns strongly influenced Mediterranean climate throughout the Holocene.

Radiocarbon dates and stratigraphic, geochemical, and pollen records reveal large-scale climate and vegetation changes influenced the eastern Mediterranean region during the Holocene (Walker *et al.* 2012). In general, high proportions of mixed deciduous pollen taxa and low $\delta^{18}O$ values in freshwater sediments and carbonates recorded during the Early Holocene (~11,700–8200 calibrated years before present, or yrs BP) indicate it was warm and humid (Jones & Roberts, 2008; Jones *et al.*, 2011; Walker *et al*., 2012). The Early-Middle Holocene boundary is defined by the 8.2 ka yrs BP (8200 yrs BP) event. This event was tied to a sudden decrease in global temperatures, as indicated by synchronous decreases in $\delta^{18}O$ and D/H in Greenland Ice Sheet cores, and correlated to hyper-arid conditions in the Adriatic, as evidenced by falling lake

levels and river discharge in the Afro-Mediterranean region (Roberts *et al*., 2011; Walker *et al*., 2012). Pollen analyses and carbonate $\delta^{18}O$ perturbations indicate that the Middle Holocene (~8200–4200 yrs BP) was a transitional period of warming but interrupted by alternating wet and dry climate phases of 200–400 years duration, on average. During the Late Holocene (~4200 yrs BP–present), the regional trend in climate was one of warming and increasing aridity demonstrated by high proportions of shrub/scrubland pollen taxa, decreases in mixed deciduous pollen taxa, and elevated $\delta^{18}O$ values (Jalut *et al.*, 2009; Combourieu-Nebout *et al*., 2014; Lončar *et al.*, 2017).

2.2.1 Hydroclimate

Global wind and weather patterns have a strong influence on temperature and hydroclimate patterns in the Mediterranean region. Systems such as the North Atlantic Oscillation (NAO), Intertropical Convergence Zone (ITCZ), and the Mediterranean Oscillation (MO or WeMO) shift position with changes in solar insolation and season creating major swings in climate conditions (Conte *et al.*, 1989; Hurrell et al., 2003; Jalut *et al.*, 2009; Benito *et al.*, 2015b). Regional circulation patterns produced by the convergence of these atmospheric systems are particularly strong controls on evaporation and precipitation in the Mediterranean (Conte *et al.*, 1989; Rohling *et al.*, 2002; Goodess & Jones, 2002; Martin-Vide & Lopez-Bustins, 2006).

Such variations in hydroclimate during the Holocene induced multiple regular flooding intervals in the Mediterranean and Adriatic regions. Here, we use the term *flooding* to refer to conditions wherein precipitation extremes cause lakes and rivers to overtop their boundaries and inundate surrounding terrestrial landscapes which are normally dry. Multiple studies (Støren *et al.*, 2010; Benito *et al.*, 2015a; Benito *et al.*, 2015b; Berger *et al.*, 2016; McClure & Podrug, 2016) have identified Holocene alluvial deposits that support the occurrence of at least 11 major

flood intervals that were synchronous across the entire Mediterranean region, and 7 flood events in the eastern Mediterranean (Benito *et al*., 2015b). One major interval of increased flooding activity in the eastern Mediterranean and Adriatic was between ~8000–6500 yrs BP (Benito *et al.,* 2015a; Benito *et al*., 2015b). Lakes in this region also experienced two major periods of hydroclimate change between ~8000–7000 yrs BP and ~4500–4000 yrs BP driven by deglaciation and solar insolation, which overlap with phases of increased flooding (Benito *et al*., 2015a). This interpretation is supported by lithological evidence from Podrug *et al.* (*in press*), which demonstrates a deepening of local lakes (10s of meters deep; Ilijanić *et al.,* 2018; Podrug *et al., in press*) between ~8000–6000 yrs BP in the Bribir-Ostrovica valley, which includes our sediment core locality. In this same area, McClure & Podrug (2016) identified the occurrence of multiple flooding events during the Middle Neolithic based on layers of calcareous tufa discovered during local excavations of Neolithic villages.

2.2.2 Bond events

Bond events were first identified in 1997 by Gerard Bond. These millennial-scale events, determined from deep sea cores and paleoenvironmental proxies, were cyclical periods of enhanced ice-rafting in the North Atlantic which began during the early Holocene and persisted until the late Holocene. At least 8 major Bond events have been identified at approximately 11,100, 10,300, 9400, 8100, 5900, 4200, 2800, and 1400 yrs BP. The ages of these Bond events reflect the time at which co-occurring oxygen isotope excursions and quantities of ice-rafted debris are recorded in sedimentary records. These events had a cyclicity close to 1500 years and durations lasting several hundred years (Bond *et al.*, 1997; Bond *et al.,* 2001; Zielhofer *et al.,* 2019).

In the Mediterranean and Adriatic, Bond events coincide with regional cooling and variable changes in regional precipitation. Oxygen isotope data from the Mediterranean links the peaks of Bond events to arid winter conditions, and the periods between Bond events to wet winter conditions (Lončar *et al*., 2017; Zielhofer *et al*., 2019). Well-dated fluvial deposits in the Mediterranean coincided with ice-rafted debris recorded in the North Atlantic, demonstrating that the peak of Bond events was synchronous with major flooding events in the eastern Mediterranean region (Bond et al., 2015a; Zielhofer *et al*., 2019).

2.3 Regional vegetation

Changes in regional arboreal vegetation distributions along the Dalmatia Coast during the Holocene reflect regional climatic perturbations and emerging agro-pastoral activity (Kaniewski *et al*., 2018). Pollen and charcoal records from multiple study sites in Croatia provide a complex and variable picture of vegetation change through the region. Descriptions of Croatian Holocene vegetation should therefore be interpreted as local, that is, within lake catchment areas for sediment records, and not emblematic of the entire eastern Mediterranean region.

Pollen records from Lake Vrana (a karstic lake on the northern Croatian Island, Cres) and Malo Jerzo (a karstic lake on the southern Croatian island, Mljet) during the last glacial period (115,000–11,700 years) indicate that coastal Adriatic and Croatian vegetation was originally dominated by mixed coniferous-deciduous forests, and that landscapes were mostly wooded (Di Rita & Magri, 2012; Lončar *et al.*, 2017). The start of Holocene warming initiated a gradual overturning of these woody forests, replaced by semi-open landscapes dominated by grasses and oak-beech woodlands. Around 8000–6000 yrs BP, vegetation became dominated by shrubland vegetation and a number of cereals and other grasses alongside the semi-dominant oak-beech

woodlands. This turnover may indicate the implementation of cultivation, burning, or grazing practices (Di Rita & Magri, 2012).

Similarly, pollen records and charcoal counts from Busuja Bay (Istrian Peninsula, Croatia along northern Dalmatia Coast) suggest a dominantly mixed deciduous-oak forest that gradually transformed to a pine-oak woodland by approximately 5000 yrs BP, possibly with the rise of agro-pastoral practices. There was a turnover in vegetation around 4250 yrs BP to salt-tolerant shrubland vegetation likely due to sea level rise and transgression across the relatively shallow northern Adriatic basin, although it may have been also encouraged by increased burning practices (Kaniewski *et al.*, 2018).

Charcoal counts from Bribir-Ostrovica valley localities indicate the presence of mixed-deciduous forests consisting of oak, ash, dogwood, pine, and buckthorn with smaller proportions of maple, juniper, hornbeam, various prune and apple trees (McClure, *under review*). These charcoal counts are approximately Middle Neolithic in age. These observations are relatively consistent with broad trends in Croatian vegetation during the Holocene (Di Rita & Magri, 2012; Lončar *et al.*, 2017; Kaniewski *et al.*, 2018).

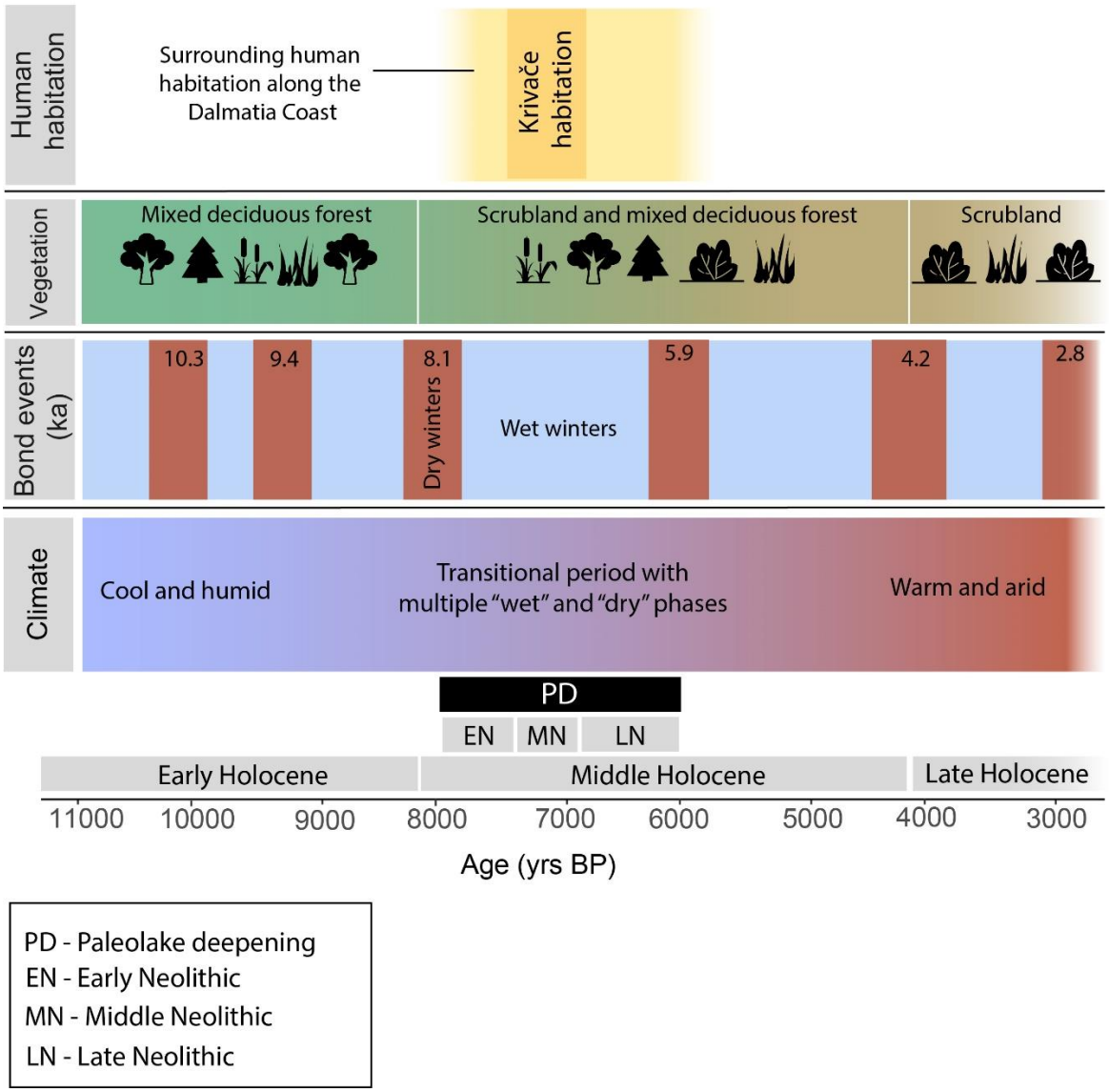

Figure 1. Summary figure of human habitation, vegetation, Bond events (ka), and general climate trends of Dalmatia Coast region during the Holocene. An interval of inferred paleolake deepening at the study site is indicated by the black box.

2.4 Study site (OSP-2)

The core OSP-2 recovered lacustrine sediments from the southeast edge of the Bribir-Ostrovica valley, approximately 20 km northwest of the city of Šibenik (McClure & Podrug,

2015; Podrug *et al.*, *in press*). During the Holocene and Neolithic, the site of OSP-2 was positioned in the middle of a large, shallow paleolake fed by the Brbišćica River and its tributaries (Podrug *et al.*, *in press*). Similar to other paleolakes in this region, the cored lake probably dried out or was drained in the modern era (Podrug *et al.*, *in press*).

OSP-2 was collected approximately 0.5 km from the Middle Neolithic site, Krivače (Fig. 2). Krivače was the nearest human habitation site to OSP-2 and was situated beside a small tributary of the Bribirčica river. Several other Neolithic habitation sites were located nearby (within ~4 km; McClure & Podrug, 2016; Podrug *et al.*, *in press*).

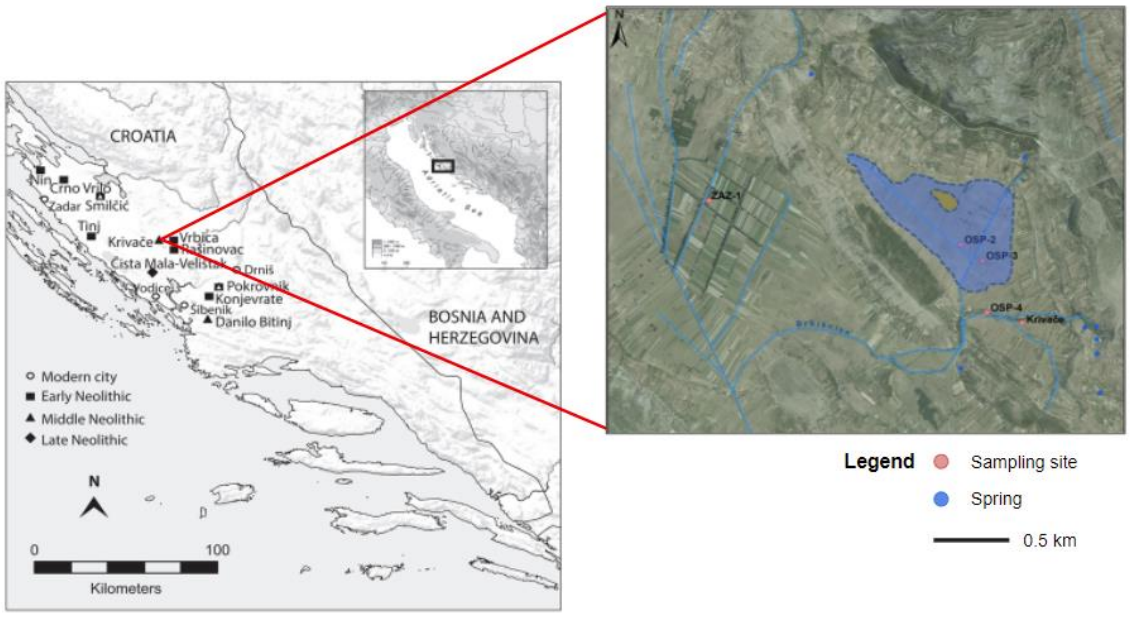

Figure 2. Geographic location of Middle Neolithic site Krivače along the Dalmatia Coast (Croatia) and an enhanced aerial image of sample site OSP-2 showing proximity to Krivače. The approximate boundaries of the paleolake are outlined and shaded in blue.

2.4.1 Human inhabitants

Archaeological studies in the Dalmatia Coast region reveal a rich and dynamic human history. During the Neolithic, human groups transitioned from nomadic, pastoralist (animal-herding) lifestyles to more settled agro-pastoral (early agrarian plant husbandry-focused)

lifestyles (Forenbaher & Miracle, 2006). This included people living in the Bribir-Ostrovica valley, who were making this transition to early agrarian lifestyles by increasing animal husbandry, adopting new tools styles, and planting new crop varieties, although the timing and pace of the transition are not well-resolved in this region (McClure & Podrug, 2015; Podrug *et al*., *in press*).

Krivače is the earliest human habitation site known in the Bribir-Ostrovica valley. It was occupied from the Early Neolithic to the beginning of the Late Neolithic (~9000–6900 yrs BP), with most recovered or described materials being Middle Neolithic in age (~7400–6900 yrs BP; McClure, *under review*; Podrug *et al*., *in press*). Habitation dates are determined by classification of ceramic and lithic typologies in combination with radiocarbon dating of excavated layers that include cultural materials such as tools, bones, plant remains, and seashells (McClure, *under review*; Podrug *et al*., *in press*).

New tools, pottery technologies, and faunal assemblages of domesticates excavated from Krivače indicate an increased reliance on agriculture, domesticated animals, and animal husbandry consistent with other Middle Neolithic sites in Croatia (McClure, *under review*; Podrug *et al*., *in press*). Here, we use the term *agriculture* to refer to early farming practices including activities such as land clearing by cutting or burning, keeping domesticated animals, and plant management by cultivating domesticated crops (Zeder, 2008). Interestingly, Krivače had a much higher proportion of cattle than observed at other sites (Podrug *et al*., *in press*), suggesting farming and husbandry practices here were at a larger scale. Plant remains from these excavations recovered 7 of the 8 founder crops that are typical of the Neolithic (einkorn, emmer, barley, pea, lentil, bitter vetch, and flax, while missing chickpea) and are appropriate for a Middle Neolithic-age settlement like Krivače (Podrug *et al*., *in press*). Plant remains of other cereals and grasses recovered suggest that inhabitants of Krivače were also processing crops or practicing other early farming activities (Podrug *et al*., *in press*; McClure & Podrug, 2016).

Excavations at other nearby Early Neolithic (Middle Holocene) sites (~6000–5000 yrs BP) revealed the development of new tools, evidence suggests both an increased regional reliance on animal husbandry and increased vegetation cutting (McClure *et al*., *in press*). Pot shards with lipid residues from milk and fermented dairy (e.g., from cheese or yogurt) have been found at these sites (McClure *et al.*, 2018). New tool styles, including sickles, also appeared alongside existing tools with different wear patterns than previously observed, indicating a shift in plant harvesting strategies and plant agriculture (McClure, *under review*; McClure *et al*., *in press*). It is likely the technology and practices of human inhabitants at Krivače followed similar developments, although further excavations are required to confirm this.

2.4.2 Lithological description

The OSP-2 core recovered dominantly lacustrine (lake) sediments, except for the modern topsoil, providing opportunity to establish a climate record for at least one paleolake in the Bribir-Ostrovica valley (Fig. 3). The deepest lithological unit (460–310 cm) is characterized as a massive gray carbonate mud with intraclasts throughout and little plant material. There is a large rock (~10 cm) between 392–397 cm of unknown lithology interrupting the core, and therefore no lithologic unit is specified for this depth horizon. The middle lithological unit (310–100 cm) is characterized by alternating layers of black and gray shale, siltstone, and mudstone interspersed with shells, gastropods, and plant material. The shallowest lithological unit (100–0 cm) is characterized by a thick package of light brown siltstone overlain by shallow layers of shale and topsoil interspersed with shells, gastropods, and plant material (Ilijanić et al., *unpublished figure*).

A preliminary record of siliciclastics and clays in OSP-2 (Fig. A1) reveals that most samples contain between 0–20% siliciclastics and clays and 0–40% sand-sized grains. Between

400–310 cm, sand and fine-sand sized grains are virtually absent, although this interval only represents 4 OSP-2 samples used in this present study. There are no other significant influxes or hiatuses in siliciclastic and clay deposition indicated by these lithological records.

3. Methods

3.1 Sample selection and preparation

Sediment cores were drilled in Croatia at study site OSP-2 (43°93'82.27" N, 15°81'30.56" E, 113 m above sea level) using a Cobre TT Eijkelkamp impact drill. 460 cm of core was collected, photographed, described, and segmented at 1 cm intervals on site. Segmented samples were bagged and labeled by project name and sample depth (Gagnon, 2021; Podrug *et al.*, *in press*). Of the 64 samples collected at the study site, 39 were selected for this study based on their approximate ages determined via radiocarbon analysis and their proximity to/overlap with the human habitation interval at Krivače identified by complementary radiocarbon analyses of sediments and archaeological artifacts by Podrug *et al.*, (*in press*) and McClure *et al.*, (*in press*). It should be noted that sampling density was greatest between 7950–6678 yrs BP and the more limited sample resolution outside this interval should be considered when making interpretations. Samples were freeze-dried to remove excess water and dry samples were weighted to approximately 10 g for extraction and chromatography.

3.2 Radiocarbon Dating

Three sediment samples were selected for radiocarbon analysis based on the type and amount of organic macroscopic material obtained at regular intervals through the sediment core.

The selected samples are from depths 195–196 cm, 298–299 cm, and 420–425 cm (sample names OSP2-195-196, OSP2-298-299, and OSP2-420-425, respectively). These samples were all classified as containing uncharred organic matter from bulk samples.

Radiocarbon analyses were performed at the Pennsylvania State University Radiocarbon Laboratory in 2017. The data were corrected following radiocarbon age dating best practices modified from Stuiver & Polach (1977). ^{14}C abundance data from the selected samples were normalized for $\delta^{13}C$ fractionation in accordance with protocols outlined by Stuiver & Polach (1977). $\Delta^{13}C$ values were prepared and measured using Accelerated Mass Spectrometer (AMS) and compared to $\delta^{13}C$ values of the original sample matter to check for fractionation during sample preparation. Comparison of these values did not indicate evidence of fractionation. Raw data from radiocarbon analysis may be found in the appendix material. An age-depth model was constructed from a calibration curve using the program OxCal. This program was used to assign ages (calibrated years before present, or cal yrs BP) to each of the dated samples. The resulting model is shown in Fig. 3.

Results from radiocarbon dating and the constructed age-depth model indicate that sedimentation rates and temporal resolution are highest at the base of the core between 495–298 cm (28.0 mm/yr). The sedimentation rate and temporal resolution is significantly less between 298–195 cm (0.23 mm/yr) and increased slightly between 195–0 cm (0.40 mm/yr). Uncertainty in the age-depth model varies between 30 and 50 years. Further information may be found in the appendix material.

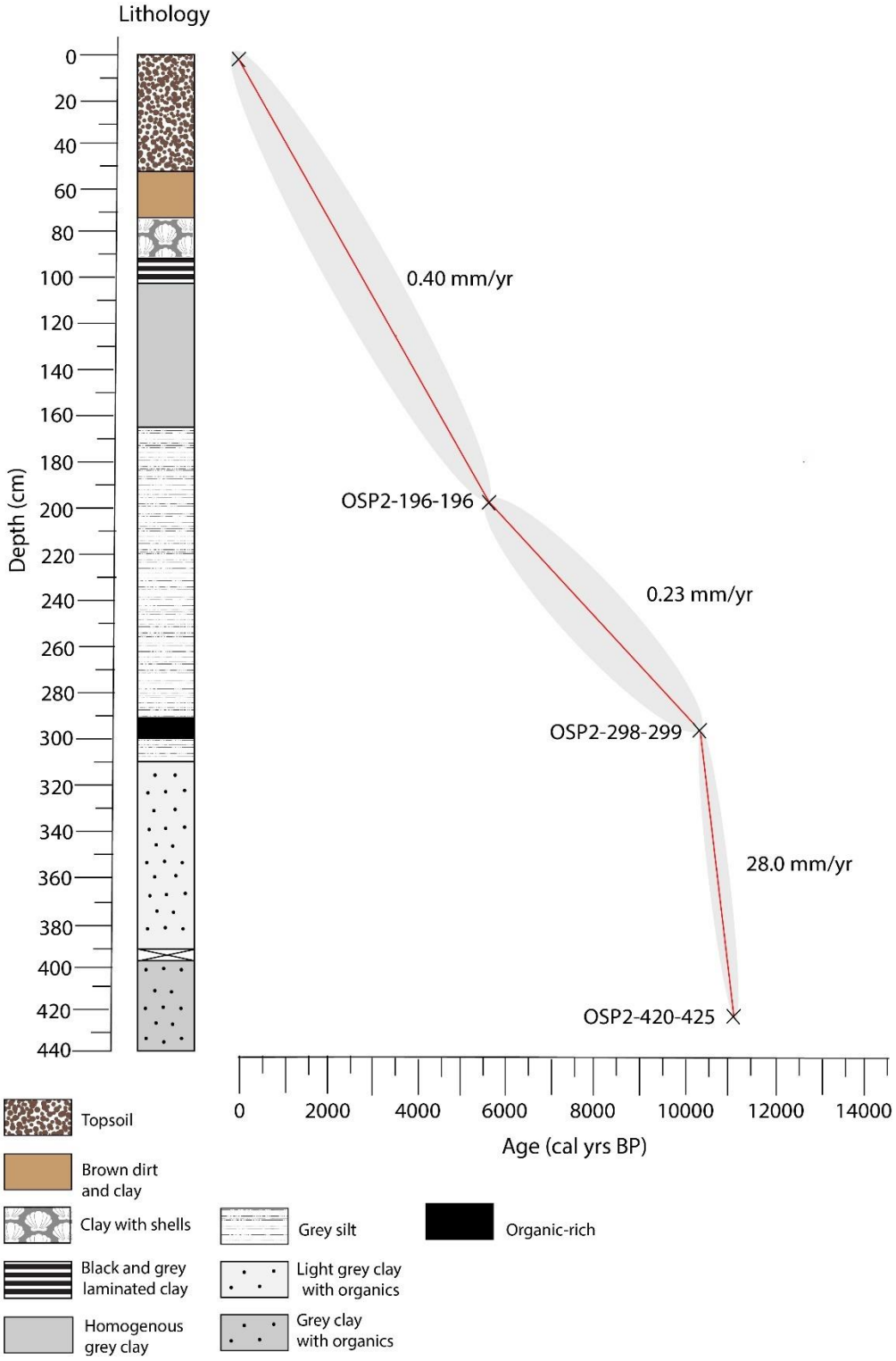

Figure 3. Age-depth profile and lithologic profile of OSP-2.

3.3 Extractions

Sediment extraction and separation methods are based on those outlined by Magill *et al.* (2015). Organics were extracted from the OSP-2 samples via a Thermo Fischer Accelerated Solvent Extraction (ASE) system with 9:1 dichloromethane (DCM) and methanol (MeOH). Extractions yielded ~50 mL of total lipid extract (TLE), of which 50% was archived. TLEs were blown down under a gentle stream of N_2 to concentrate compounds before separation into aliphatic (F1), aromatic (F2), and polar (F3) fractions.

3.4 Chromatography

Concentrated TLEs were separated into three fractions via a Dionex ASE system. ASE cells were constructed with multiple layered stationary phases as outlined in Magill *et al.* (2015). F1, F2, and F2 fractions were eluted with 100% hexane, 9:1 hexane and DCM, and 7:3 DCM and MeOH, respectively. F1 and F2 fractions were blown down under a gentle stream of N_2 and transferred to GC vials for further analysis. F3 fractions were archived.

3.5 GC-MS analysis

N-alkanes in fraction F1 were identified using a Thermo Scientific Trace 1320 Gas Chromatograph (GC) coupled to a Thermo Scientific ISQ 7000 Single Quadrupole Mass Spectrometer (MS) at the Pennsylvania State University. F1 fractions were injected via split-splitless injector (320°C) operating in splitless mode onto an RTX-5 29.2-m column (0.236-mm internal diameter, 0.25-μm film thickness). The oven temperature started at 40°C for 1 minute

and then was ramped at 7°C/min to 320°C and held for 10 minutes. Samples were run in full scan mode. *N*-alkanes were identified using mass spectra and comparison to retention times from EPA 610+ C_9–C_{40} authentic *n*-alkane standards.

PAHs in fraction F2 were identified using the same GC–MS instrument as above. The oven temperature program started at 90°C for 1 minute and then was ramped at 15°C/min to 150°C, held for 0 minutes, and then ramped n at 4°C/min to 320°C and held for 0 minutes. Samples were run in selected ion monitoring (SIM) mode. PAH compounds were identified using mass spectra and comparison to retention times from authentic PAH standards.

3.6 Quantifications

Both compound classes were quantified using 5-point calibration curves from authentic standard suites. Response factors (RFs) were extracted from calibration curves and used in the following equations to calculate i) the compound mass (ng) per mass of organic carbon (g), and ii) the compound mass (ng) per mass of sample (g dry weight), where A refers to the compound area:

$$i.\ \frac{Mass\ of\ compound\ (ng)}{Mass\ of\ sample\ OC\ (g)} = \frac{RF\ \left(\frac{ng}{A(counts * \text{minute})}\right) * A(counts * minute) * \left(\frac{100\ \mu L}{1\ \mu L}\right) * (\frac{1}{0.5})}{Sample\ weight\ (g) * \%TOC}$$

$$ii.\ \frac{Mass\ of\ compound\ (ng)}{Mass\ of\ sample\ (g)} = \frac{RF\ \left(\frac{ng}{A(counts * \text{minute})}\right) * A(counts * minute) * \left(\frac{100\ \mu L}{1\ \mu L}\right) * (\frac{1}{0.5})}{Sample\ weight\ (g)}$$

The equations vary for *n*-alkanes and PAHs to account for differences in the volume of solvent used for the injection ratio of each compound class and correct for the portion of extracts archived (1/2). Further information about these quantification steps may be found in the appendix material.

3.7 Geochemical methods

Prior work determined total organic carbon (%TOC), total calcium carbonate (%$CaCO_3$), $\delta^{13}C_{org}$ (organic carbon isotope), $\delta^{13}C_{carb}$ (carbonate carbon isotope), and $\delta^{18}O_{carb}$ (carbonate oxygen isotope) values. All data were measured at the Yale Analytical and Stable Isotope Center. Geochemical data was collected and measured using an Elemental Analyzer Isotope Ratio Mass Spectrometer (EA-IRMS).

%TOC and %$CaCO_3$ were determined by following protocols as outlined by Carvajal-Ortiz & Gentzis (2015). Sediment samples were first freeze-dried, weighed, powdered, and small shells were removed. Dry sediment samples were then acidified in 1N HCl to remove carbonate materials, rinsed, freeze-dried, and weighed again to calculate the mass lost during acidification. Samples were pyrolyzed, and CO_2 from combustion was measured on the EA-IRMS using response factors determined from calibrated standards with known %TOC values. %$CaCO_3$ for each sample was calculated by comparing sample masses before and after acidification according to the following equation:

$$\%CaCO_3 = \frac{[Initial\ sample\ weight\ (g) - final\ sample\ weight\ (g)]}{Initial\ sample\ weight\ (g)} * 100$$

%TOC for each sample was calculated by correcting measured masses for mass lost during acidification and the IRMS measurement of %TOC according to the following equation:

$$\%TOC = \left(1 - \frac{\%CaCO_3}{100}\right) * \%TOC_{IRMS}$$

Carbon isotopes ($\delta^{13}C_{org}$ and $\delta^{13}C_{carb}$) and oxygen isotopes ($\delta^{18}O_{carb}$) were measured on the EA-IRMS and normalized to the international carbon isotope standard Vianna Pee Dee Belemnite (VPDB). All isotope measurements were calibrated against an in-house standard and isotope values are reported in permil (‰) delta notation. The measurement precision of the EA-IRMS was determined by running replicates of 3 standards with known $\delta^{13}C_{org}$ values. The average precision (standard deviation of $\delta^{13}C_{org}$) across all runs was 0.37‰ and the average accuracy (average of differences) was -0.124‰.

3.8 Charcoal methods

Charcoal data were collected from the OSP-2 core as part of a senior thesis project at the Pennsylvania State University by Catherine Gagnon under the guidance of Dr. Katherine Freeman. Five macrocharcoal samples were collected for macrocharcoal analysis and counted using a stereomicroscope and hand-counter. Charcoal particles were quantified using the automated counting software ImageJ and calibrated against the intermediate size fraction (125-177 μm) of the charcoal samples. Samples are Middle Neolithic (~8300–6400 yrs BP) in age, as determined by radiocarbon dating, and overlap the Krivače habitation interval (~7400–6900 yrs BP).

3.9 Pollen methods

Pollen data was collected from the OSP-2 core as part of a senior thesis project at the Pennsylvania State University by Matt Wileyto under the guidance of Dr. Sarah Ivory. 10 pollen samples were collected for analysis. Due to preservational biases and sparse organic matter, only 1 sample was collected from the inferred habitation interval at Krivače (~7400–6900 yrs BP).

Pollen counts were extracted from sediment samples using standard methods outlined in Faegri & Iversen (1964) by hydrofluoric acid digestion and acetolysis. Counts were calibrated by adding *Lycopodium* spores of known concentrations and pollen was counted using digital image analysis. Pollen types were identified under a standard microscope, and abundances and concentrations were calculated manually. Pollen counts were determined to be Early to Middle Neolithic (~9000–5500 yrs BP) in age by radiocarbon dating, and they overlap the Krivače habitation interval (~7400–6900 yrs BP).

4. Results

4.1 *N*-alkanes

4.1.1 Distribution

N-alkane abundances between ~8000-6000 yrs BP are elevated, and sharply decrease before and after this interval. Within the ~8000-6000 yrs BP interval, there are two abundant *n*-alkane groups. The group with the higher abundance consists of even-numbered short-chain *n*-alkanes, ranging from C_{16} to C_{22} with C_{18} as the most abundant (Fig. 4A). The second most abundant group consists of odd-numbered long-chain plant waxes, ranging from C_{27} to C_{35} with C_{29} as the most abundant (Fig. 4B). In this interval, the even, short-chain *n*-alkanes are approximately 2-3 times more abundant than their odd, long-chain homologues.

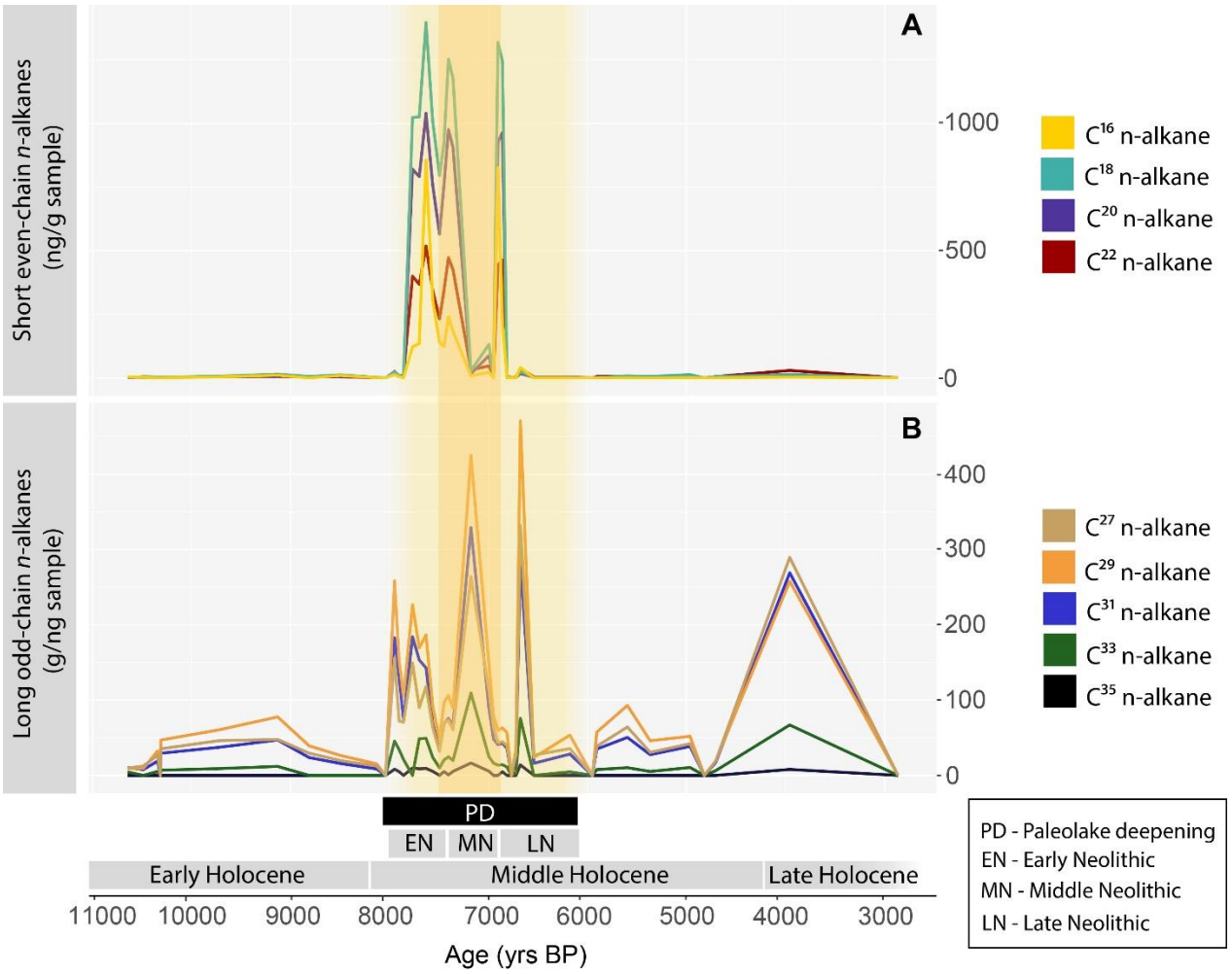

Figure 4, A-B. N-alkane distributions across the study interval, divided into two modes. Panel A: Distribution of short-chain even-numbered n-alkanes (C_{16}–C_{22}; ng/g). Panel B: Distribution of long-chain odd-numbered n-alkanes (C_{27}–C_{35}; ng/g). The dark yellow box indicates the Krivače habitation window, and the yellow shaded box indicates the window of surrounding habitation along the Dalmatia Coast. The interval of inferred paleolake deepening is indicated by the black box.

4.1.2 Ratios

N-alkane ratios offer additional ways to assess the identities, sources, or specific groupings of vegetation in samples. The carbon preference index, or CPI (Bray & Evans, 1961), is often interpreted as a measure of the thermal maturity of *n*-alkanes. Here, we define CPI as a

measure of the dominance of i) long-chain alkanes (CPI_{long}) and as a measure of the dominance of ii) short-chain alkanes (CPI_{short}), where C_n is the peak area of compounds with chain length = *n*:

$$i.\ CPI_{long} = \left[\left(\frac{\sum C_{27-33odd}}{\sum C_{26-33even}}\right) + \left(\frac{\sum C_{27-33odd}}{\sum C_{28-34even}}\right)\right] * 0.5$$

$$ii.\ CPI_{short} = \left[\left(\frac{C_{16} + C_{18}}{C_{15} + C_{17}}\right) + \left(\frac{C_{16} + C_{18}}{C_{17} + C_{19}}\right)\right] * 0.5$$

Increased CPI_{short} values represent a greater abundance of even compounds. These values can reflect increasing thermal degradation from burning activity (Weisenberg *et al.*, 2009), but alternatively could indicate increased input from biological sources that make even alkanes in this length range (i.e., algae, bacterial, or some plants). We find CPI_{short} values for OSP-2 varied significantly between 1–45 across the study interval (Fig. 5A). CPI_{short} was low (1–4) between ~11,000–7800 yrs BP. From ~7800–6800 yrs BP, CPI_{short} values increased by an order of magnitude and varied between 18–45. From 6800 yrs BP–present, CPI_{short} values returned to low and less variable values (1–3).

CPI_{long} values >1 indicate biological signatures dominated contributions to sedimentary archives. CPI_{long} values <1 indicate biological signals were thermally altered or degraded in sedimentary archives, including input from petroleum sources. CPI_{long} values for OSP-2 are all >1, except for 1 sample at 6769 yrs BP, which has a value just below 1 (Fig. 5B).

The average chain length, or ACL, is a ratio used to track shifting contributions of vegetation types (Freeman & Pancost, 2014; Weisenberg *et al.*, 2009; Diefendorf & Freimuth, 2017). Two applications includes distinguishing contributions of short or long-chain *n*-alkane inputs (ACL_{total}; Weisenberg *et al.*, 2009) and C3 or C4 sources of *n*-alkanes (ACL_{long}; Freeman & Pancost, 2014; Diefendorf & Freimuth, 2017). ACL_{total} and ACL_{long} are defined by the following equations where C_n is the peak area of compounds with chain length = *n* and *n* = 14-35:

$$i.\ ACL_{total} = \frac{(\sum z_n * n)}{\sum z_n}$$

$$ii.\ ACL_{long} = \frac{(27 * C_{27}) + (29 * C_{29}) + (31 * C_{31}) + (33 * C_{33}) + (35 * C_{35})}{C_{27} + C_{29} + C_{31} + C_{33} + C_{35}}$$

ACL_{total} values reveal trends in the proportions of long and short-chain *n*-alkanes over time. Weisenberg *et al.* (2009) reported decreasing ACL_{total} values as a result of heating experiments, which can cause thermal degradation whereby increasing temperatures amplify cracking of carbon bonds, decreasing chain lengths (Weisenberg *et al*., 2009; Polissar *et al*., 2021). However, any process that produces short-chain homologs would lower ACL_{total} values. ACL_{total} values for OSP-2 vary between 19–28 (Fig. 5C). ACL_{total} is ~27 between 11,000–7900 yrs BP. Between 7900–6800 yrs BP, ACL_{total} values drop to and oscillate around ~20 for almost 1000 years. This interval of lower ACL_{total} values mirrors the drop in CPI_{long} values (Fig. 7D) across the same interval with a slightly amplified appearance. At 6800 yrs BP, ACL_{total} returns to ~27 and remains stable up to the modern era.

In studies of savannah ecosystems, especially in eastern Africa, ACL_{long} values >31 indicate contributions from C4 grasses, whereas ACL_{long} values <31 indicate contributions from woody and non-woody C3 plants (Freeman & Pancost, 2014; Diefendorf & Freimuth, 2017). In this study, ACL_{long} values were all below 31 (Fig. 5D).

The aquatic plant index, or pAQ, is a ratio used to determine aquatic or terrestrial sources of *n*-alkanes. pAQ is defined by the equation (Fiken *et al*., 2000) where C_n is the peak area of compounds with chain length = *n:*

$$pAQ = \frac{C_{23} + C_{25}}{C_{23} + C_{25} + C_{29} + C_{31}}$$

Low pAQ values, between 0-0.23, indicate significant contributions from terrestrial plants. Intermediate pAQ values, between 0.23-0.61, indicate contributions from emergent

macrophytes. Highest pAQ values, between 0.48-1, indicate contributions from submerged or floating macrophytes (Ficken *et al*., 2000). Due to the overlap in ranges between emergent and submerged/floating macrophytes, we combined these categories together such that pAQ values between 0.23-1 indicate contributions from aquatic plants that were some combination of submerged and/or floating macrophytes. pAQ values for OSP-2 oscillate above and below 0.23 throughout the entirety of the core but are dominantly >0.23 (Fig. 5E). While pAQ has not been explicitly examined against the deepening of lacustrine environments, greater lake depths and volumes should allow for greater species richness in lakes (Hobæk *et al.,* 2002) and increase the distance between the core location and the paleo shoreline, which would coincide with increasing pAQ values. However, profiles of pAQ and water depth at Lake Qinghai (on the Qinghai-Tibet Plateau) reported in Liu *et al.* (2016) do not show strong covariance between pAQ and water depth. Specific sampling experiments comparing *n*-alkanes and pAQ at a range of lake depths in multiple lake settings (i.e., open and closed basins, lakes of different areas, volumes, and seasonal patterns) could help address this question. A summary table with all these ratios may be found in the appendix material.

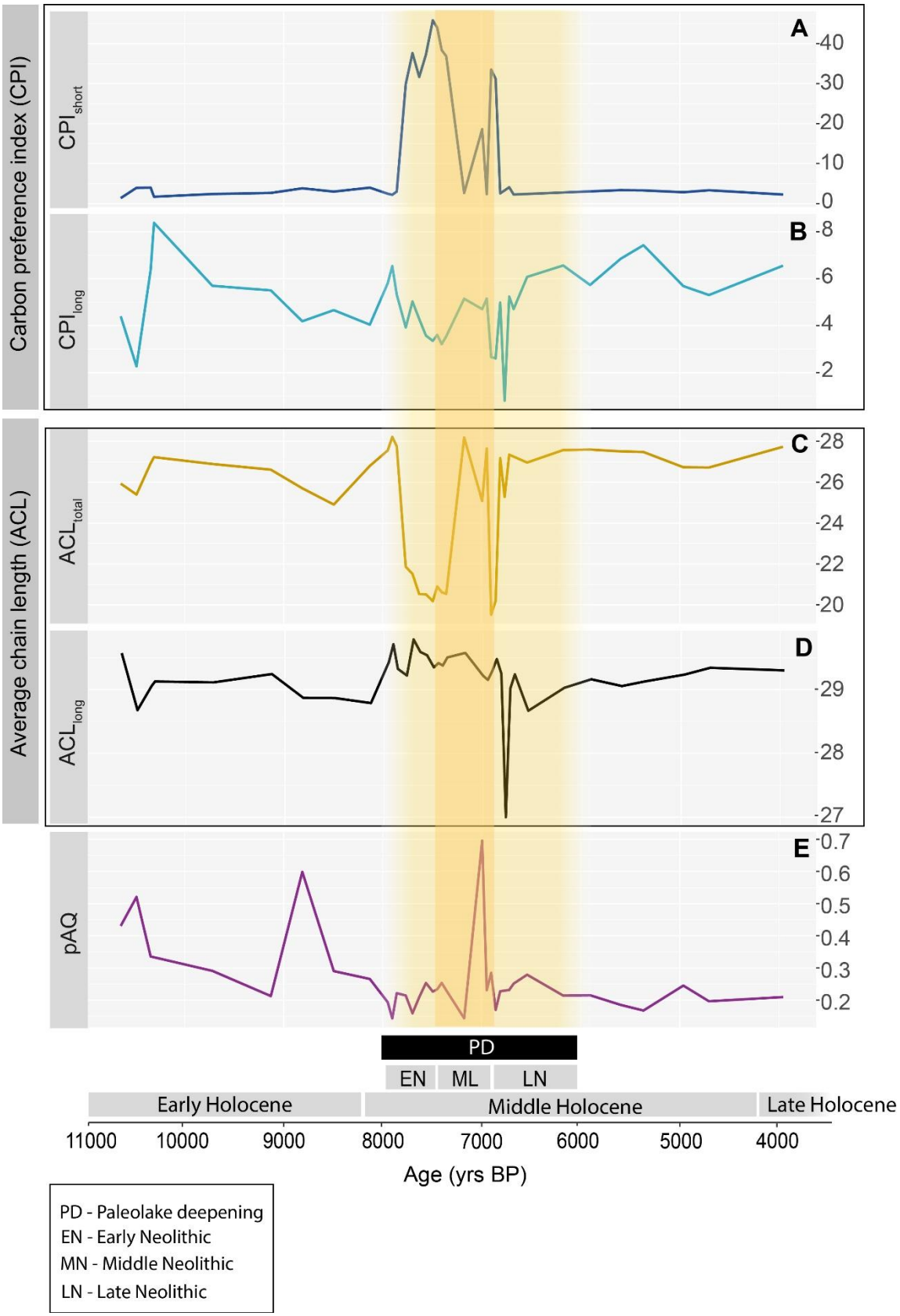
Carbon preference index (CPI)
CPI short
CPI long
A
B
40
30
20
10
0
8
6
4
2
Average chain length (ACL)
ACL total
ACL long
C
D
28
26
24
22
20
29
28
27
pAQ
E
0.7
0.6
0.5
0.4
0.3
0.2
PD
EN
ML
LN
Early Holocene
Middle Holocene
Late Holocene
11000
10000
9000
8000
7000
6000
5000
4000
Age (yrs BP)
PD - Paleolake deepening
EN - Early Neolithic
MN - Middle Neolithic
LN - Late Neolithic

Figure 5, A-E. Plots of n-alkane ratios including CPI (CPI_{long} and CPI_{short}), ACL (ACL_{long} and ACL_{total}), and pAQ across the study interval. Panels A and B: Distributions of CPI_{long} and CPI_{short}. CPI_{short} at ~6800 yrs BP and between ~6500–5900 yrs BP could not be calculated due to zero values for short-chain even-numbered n-alkanes. Panels C and D: Distributions of ACL_{long} and ACL_{total}. Panel E: Distribution of aquatic plant index (pAQ) values. The dark yellow box indicates the Krivače habitation window, and the yellow shaded box indicates the window of surrounding habitation along the Dalmatia Coast. The interval of inferred paleolake deepening is indicated by the black box.

4.2 PAHs

4.2.1 Distribution

In this study, we focused on the fire-associated parent PAHs phenanthrene, fluoranthene, and pyrene, and the source-indicator ratios involving alkylated PAHs retene and methylated homologs of phenanthrene. Parent PAH abundances show a similar increase to the *n*-alkanes between ~8000–6000 yrs BP (Fig. 6). Within this interval, the largest spike in abundances were coeval with the Krivače habitation interval. Abundances are slightly elevated but noisy before this interval, and mostly drop off after this interval. Of these compounds, pyrene was approximately 2 times more abundant than the other parent PAHs between ~8000–7000 yrs BP.

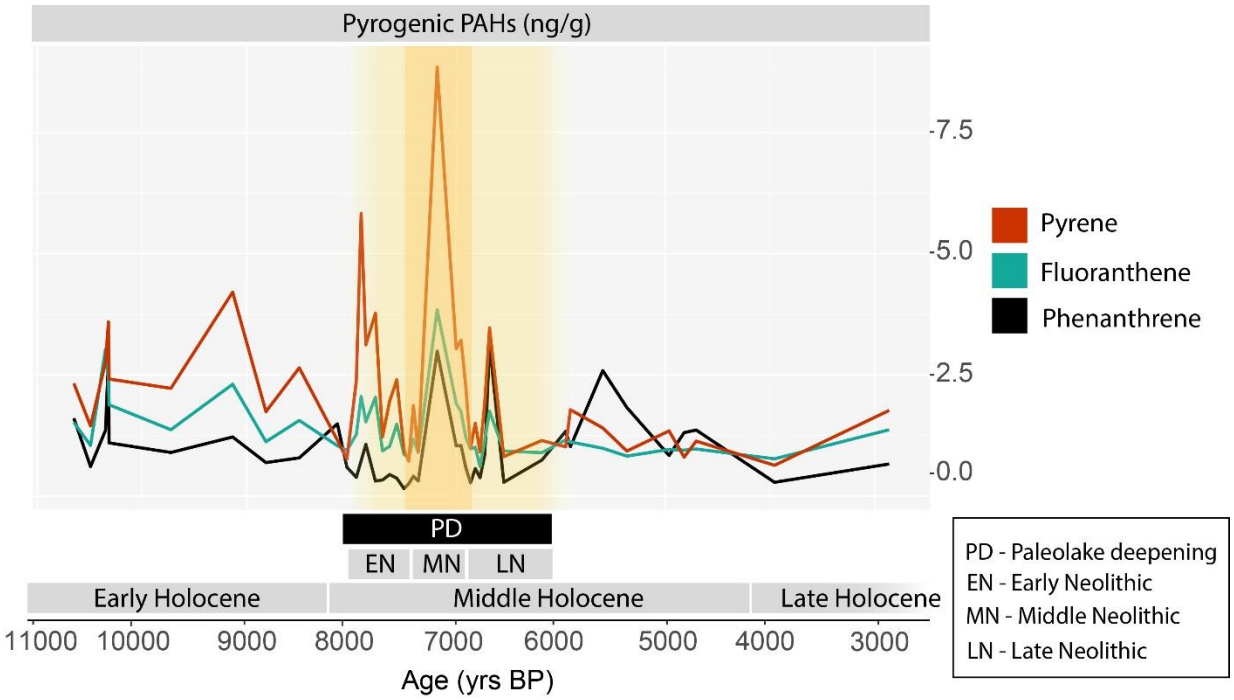

Figure 6. Distribution of pyrogenic PAHs (phenanthrene, fluoranthene and pyrene; ng/g) across the study interval. The dark yellow box indicates the Krivače habitation window, and the yellow shaded box indicates the window of surrounding habitation along the Dalmatia Coast. The interval of inferred paleolake deepening is indicated by the black box.

Parent pyrogenic PAHs normalized to terrestrial vegetation allows a clearer interpretation of the fire record by accounting for fuel load due to changing biomass, in addition to transport and preservation factors (Denis *et al.*, 2012; Karp *et al.*, 2018; Denis *et al.*, 2021). We normalized pyrene, the most abundant pyrogenic PAH, against the C_{29} *n*-alkane and the alkylated PAH retene. The C_{29} *n*-alkane was selected for normalization as the most abundant odd-numbered long-chain plant wax as an indicator of terrestrial biomass. Normalization against the C_{29} *n*-alkane shows no enhanced pyrogenic signal (Fig. 7A), in contrast to the non-normalized parent PAH distribution (Fig. 6).

We also normalized against retene because plant *n*-alkanes, including C_{29}, are not abundant in many conifers (Diefendorf *et al.*, 2014). Conifers contain abundant diterpenoid compounds, which distinguish conifer inputs from angiosperm vegetative sources (Diefendorf *et*

al., 2014). Retene is produced from degradation of diterpenoids and a marker of burn products from conifers (Diefendorf *et al.*, 2014; Karp *et al.*, 2020), and thus we use retene to normalize against any potential conifer biomass sources here. Normalization against retene does not show an enhanced pyrogenic signal (Fig. 7B).

To further assess preservational signals, total pyrogenic PAH abundances were normalized against total PAH abundances. If the normalization preserves the original elevated pyrogenic PAH values (Fig. 7C), then we can assume that increased pyrogenic PAHs reflect an increased influx to the lake sediments and not an artifact of enhanced preservation changes. Resulting values (Fig. 7C) exhibit a strikingly similar distribution trend to the *n*-alkanes with significantly elevated values between ~8000–6000 yrs BP.

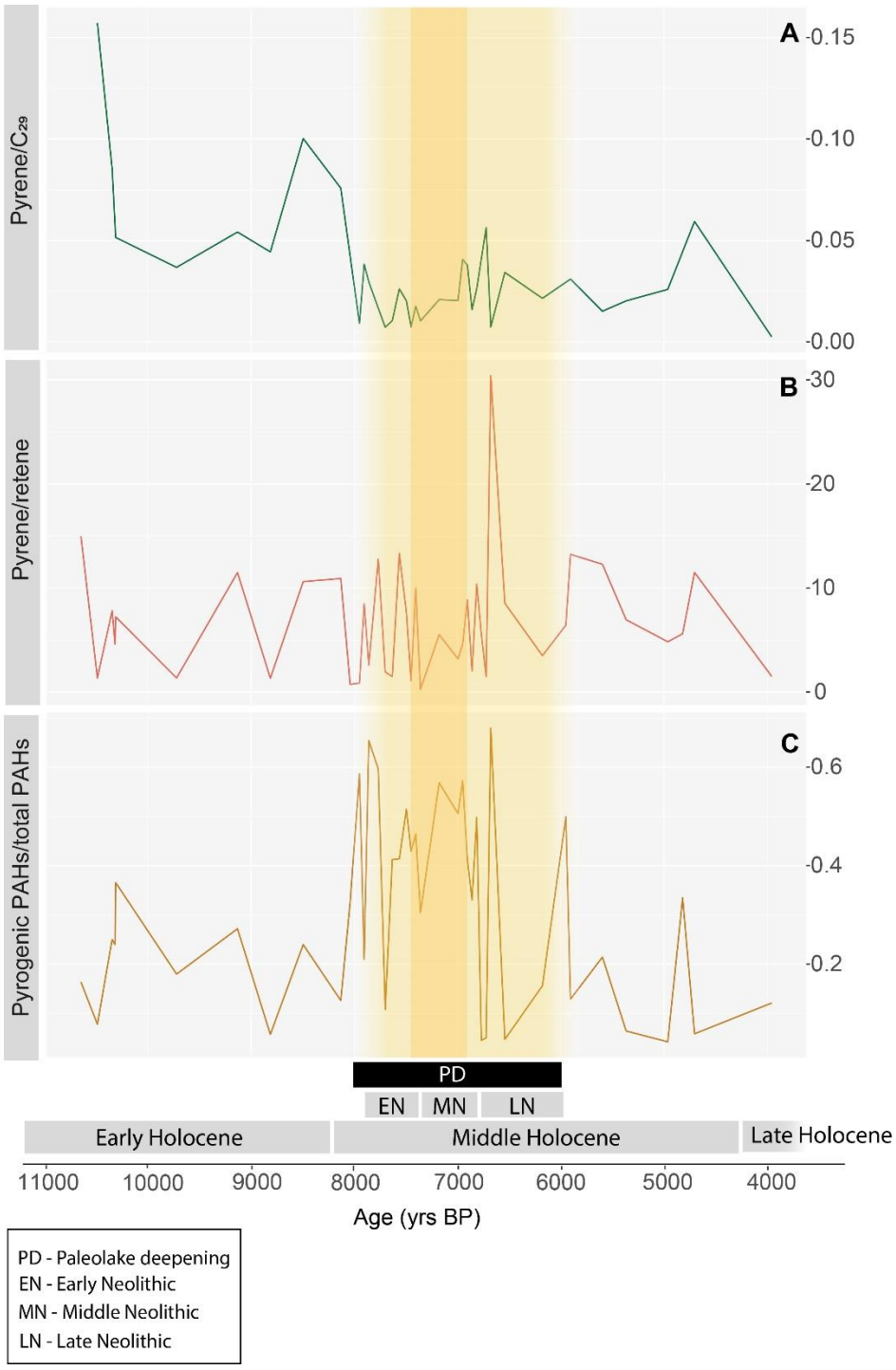

Figure 7, A-C. Normalized PAH distributions across the study interval. Panel A: Distribution of pyrene (ng/g) normalized to the C_{29} n-alkane (ng/g). One sample was removed at 6967 yrs BP due to a zero value for C_{29}. Panel B: Distribution of pyrene (ng/g) normalized to retene (ng/g). Panel C: Distribution of pyrogenic PAHs (ng/g) normalized to the total amount of PAHs (ng/g). The dark yellow box indicates the Krivače habitation window, and the yellow shaded box indicates

the window of surrounding habitation along the Dalmatia Coast. The interval of inferred paleolake deepening is indicated by the black box.

4.2.2 Ratios

Molecular PAH ratios can help identify fuel sources for pyrogenic PAHs (Yunker *et al.*, 2002). This study focused on the retene/3-ring ratio and the alkylated PAH derivative index (APDI) to further assess these parameters.

The retene/3-ring ratio is a measure to identify changes in the type of plant community burned, and is defined by the following equation where Ret = retene, Phen = phenanthrene, and Anth = anthracene represent the peak areas of each compound:

$$\frac{Retene}{3-ring} = \frac{Ret}{Ret + Phen + Anth}$$

Values >0.1 indicate the burning of woody gymnosperms (conifers), whereas values <0.1 indicate the burning of woody angiosperms (Simoneit, 1997; Miller *et al.*, 2017; Karp *et al*., 2020). Values for OSP-2 are almost entirely >0.1 and yield the highest values (>0.6) between ~8000–6000 yrs BP (Fig. 8A). Values prior to 8000 yrs BP are mostly elevated, but variable. Values after 6000 yrs BP drop to below 0.1, with the exception of 1 point near the modern.

The APDI is a descriptive PAH index developed by Karp *et al*., (2020) determined from a series of controlled burning experiments. The APDI metric can be used to distinguish pyrogenic from petrogenic/coniferous PAH sources and is defined by the equations:

$$APDI = [f''(x) - f'(2)]\ for\ a\ parabolic\ curve$$

$$f(x) = ax^2 + bx + c$$

$$fit\ to\ a\ normalized\ distribution\ of\ alkylated\ PAHs\ (0{,}1{,}2{,}3\ methyl\ groups)$$

APDI values <0, or results that are concave and increasing, indicate petrogenic or coniferous sources. APDI values >0, or results that are convex and decreasing, indicate pyrogenic sources

(Blumer & Youngblood, 1975; Laflamme & Hites, 1978; Stogiannidis & Laane, 2015; Kappenberg *et al.*, 2019; Karp *et al.*, 2020). Negative values could also be associated with PAH released from soil, as weathering can increase relative amounts of alkylation in PAH compounds (Johnsen *et al.*, 2005; Zhang *et al.*, 2006; Karp *et al.*, 2021). APDI values for OSP-2 are mostly <1 between ~8000-6500 yrs BP, and mostly >1 before and after this interval (Fig. 8B). A more thorough summary of these ratios may be found in the appendix material.

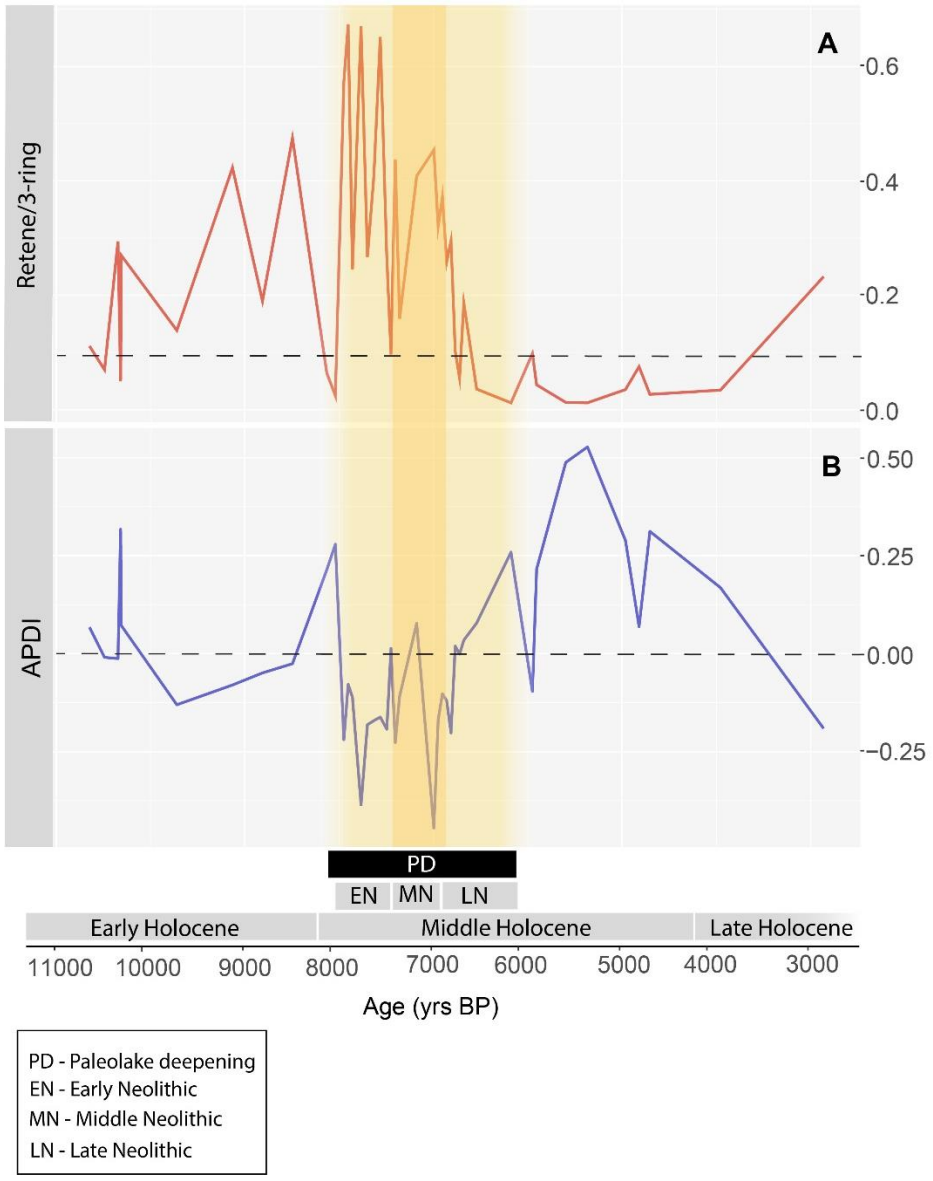

Figure 8, A-B. Figure displaying PAH indices including retene/3-ring ratio and APDI across the study interval. Panel A: Distribution of retene ratio values. Panel B: Distribution of APDI values. The dark yellow box indicates the Krivače habitation window, and the yellow shaded box indicates the window of surrounding habitation along the Dalmatia Coast. The interval of inferred paleolake deepening is indicated by the black box.

4.3 Previous OSP-2 data

4.3.1 Lithologies

Lake sediments are valuable paleoenvironment and paleoclimate archives, as they record changes in water and sediment inflow from the surrounding landscape (Schnurrenberger et al., 2003; Podrug *et al.*, *in press*). Changes in lithologies and fossil assemblages through the core reveal a persistent lake history from its origin (~11,200 yrs BP) until it dried in the modern period.

Of note is the shift in lithologies at 310 cm from a majority carbonate to siliciclastic units coupled with changes in ostracod assemblages, suggesting changes in climate affected the lake environment and depositional conditions. Previous lithological analysis by Podrug *et al*. (*in press*) suggests that the lake was shallow and the climate was cool during its earliest phase, then the lake progressively deepened, indicated by deposition of authigenic calcite, then shallowed again over time while the climate consistently warmed. The maximum depth of the paleolake was likely no more than 6 m deep based on geomorphology of the valley and microfossil faunal assemblages found at the site (Podrug *et al.*, *in press*).

4.3.2 Geochemical records

Trends in %TOC and $\%CaCO_3$ can be used to interpret organic and inorganic accumulations of carbon and changes in oxygen content in the lake environment. Here, %TOC

and %$CaCO_3$ demonstrate intervals of strong negative covariance with one another, which may indicate intermittent anoxic or low oxic conditions (Nioti *et al.,* 2013). Intervals lacking strong correlation between the two records likely reflect different sources of organic and inorganic carbon (Nioti *et al.,* 2013). %TOC varies between 0 and 7.3 wt% (Fig. 9). There is a sharp increase to 7.3 wt% at ~10,300 yrs BP coinciding with a shift to dark, organic-rich lithologies before dropping back to 1 wt% by ~10,200 yrs BP. From ~10,200–4700 yrs BP, %TOC is relatively stable between 0 and 2%. %TOC increases to 4.7 wt% by ~3900 yrs BP then decreases to 1.7 wt% at ~2800 yrs BP.

The trend in %$CaCO_3$ mirrors %TOC and varies between 48 and 98 wt% (Fig. 9). There is a sharp decrease to 72.2 wt% at ~10,400 yrs BP and again to 48.4 wt% at ~10,300 yrs BP (the lowest value of the dataset) before increasing back to 95.4 wt% by ~10,200 yrs BP. Between ~10,200–4700 yrs BP, %$CaCO_3$ is stable between 84–98 wt%.

In the interval of habitation, ~8000–6000 yrs BP, %TOC exceeds 2 wt% near ~8000 yrs BP, and remains high but variable to ~6000 yrs BP, before dropping to 1 wt% and lower after ~6000 yrs BP (Fig. 10). In contrast, %$CaCO_3$ does not reveal as significant a trend across the ~8000–6000 yrs BP interval (Fig. 10). There is a slight decrease near to 85 wt% at two points near ~8000 yrs BP, but all other values but one between ~8000–6000 yrs BP remain high, 91–98 wt%. It should be noted that elevated %$CaCO_3$ can dilute %TOC values. Therefore, %TOC values should also be interpreted against other geochemical parameters (i.e., clay accumulation rate).

Organic carbon isotope ($\delta^{13}C_{org}$) values generally mirror %TOC and vary between –28.8‰ and –26.3‰ (Fig. 9). There is a noticeable decrease in $\delta^{13}C_{org}$ between ~10,600–9400 yrs BP and between ~4800 yrs BP and the present, although these trends may be influenced by low sampling resolution across these intervals. The absence of any noticeable patterns in either the $\delta^{13}C_{org}$ or %TOC records across the Krivače habitation interval record does not support a strong

relationship between organic matter input or preservation and human activity. Inorganic (carbonate) carbon isotope ($\delta^{13}C_{carb}$) values incrementally decrease across the study interval (Fig. 9). $\delta^{13}C_{carb}$ decreases from –0.51‰ to –6.46‰ between ~10,600–8900 yrs BP. Values stabilize around -6‰ from ~8900–5400 yrs BP. There is a slight decrease to –8.74‰ at ~4700 yrs BP followed by an increase to –6.26‰ at ~2800 yrs BP.

Carbonate mineral oxygen isotope ($\delta^{18}O$) values record changes to both local temperature and hydroclimate conditions. The $\delta^{18}O$ values generally trend negative and show a two-phase stepwise decrease across the study interval, while covarying with $\delta^{13}C_{carb}$ (Fig. 9). In the first phase, $\delta^{18}O$ increased from –4.2‰ to –2.82‰ between ~10,600–9400 yrs BP before decreasing again to –5.27‰ by ~7800 yrs BP. The second phase was marked by another $\delta^{18}O$ increase from –5.27‰ to –3.9‰ between ~7800–6600 yrs BP before decreasing to the lowest $\delta^{18}O$ value –6.23‰ by ~3900 yrs BP. There was a slight increase to –5.09‰ between ~3900–2800 yrs BP. Covariation between $\delta^{18}O$ and $\delta^{13}C_{carb}$ values are consistent with primary carbonate precipitation in a semi-open (partially restricted) lake basin with a long residence time (Talbot, 1990) and a reflect a common carbon source. Further climatic interpretation of the $\delta^{18}O$ record requires caution because oxygen isotopes are influenced by changes in both temperature and precipitation, which is further complicated by the highly variable Mediterranean hydroclimate.

4.3.3 Charcoal data

This preliminary dataset demonstrates an increase in counts across the habitation interval, from 250 μm at ~8600 yrs BP to a peak value of 851 at ~6700 yrs BP (Fig. 9). Counts decrease incrementally to 160 μm by ~6400 yrs BP. The high peak count value during the habitation of Krivače tentatively reflects a human-driven signal, although many more charcoal counts across this study interval are required to support this interpretation.

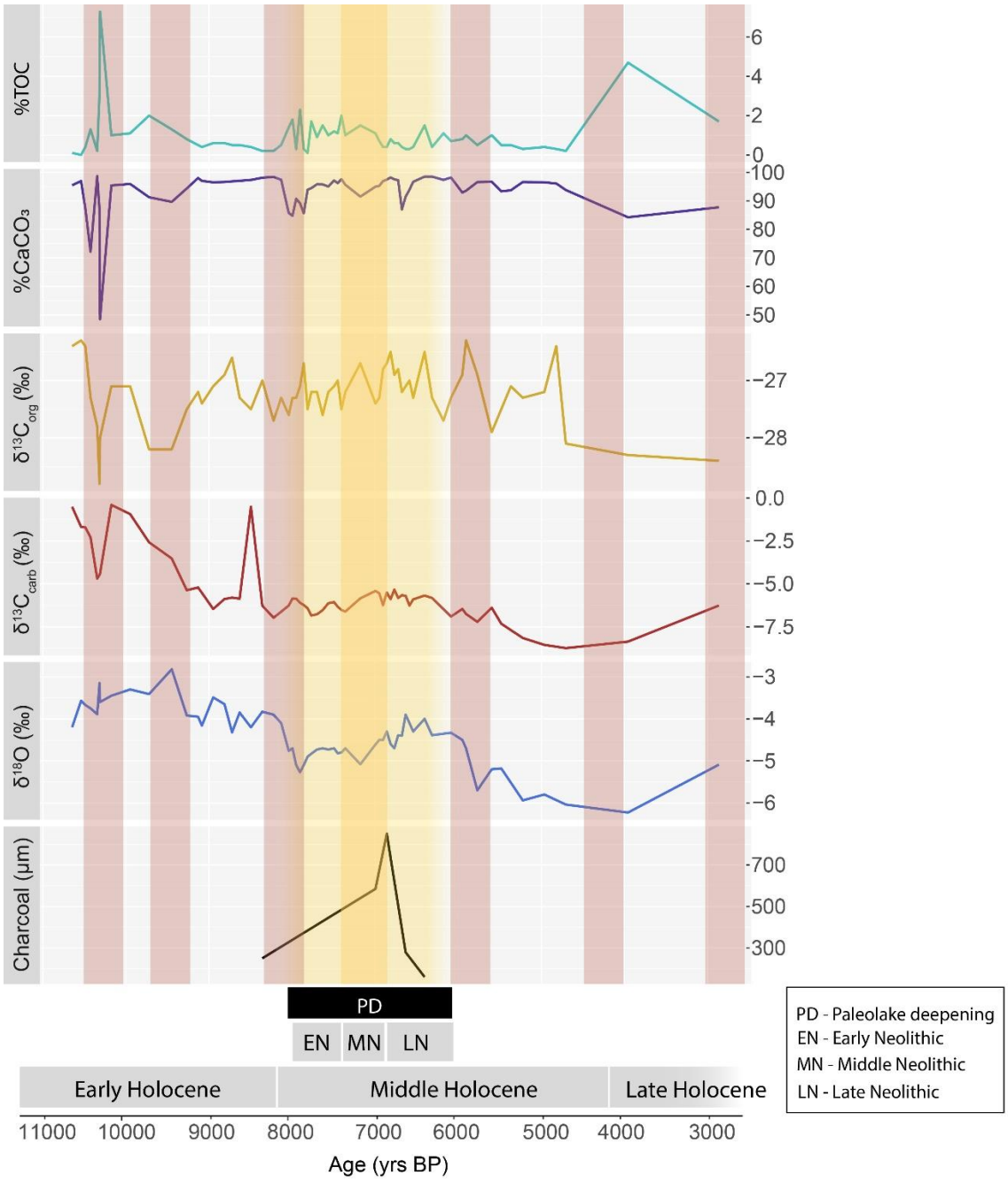

Figure 9. Geochemical profiles of %TOC, %$CaCO_3$, $\delta^{13}C_{org}$ (‰), $\delta^{13}C_{carb}$ (‰), $\delta^{18}O$ (‰), and charcoal counts (µm) across the study interval plotted against sample age (yrs BP). The dark yellow box indicates the Krivače habitation window, the yellow shaded box indicates the window of surrounding habitation along the Dalmatia Coast, and red boxes indicate Bond events. The interval of inferred paleolake deepening is indicated by the black box.

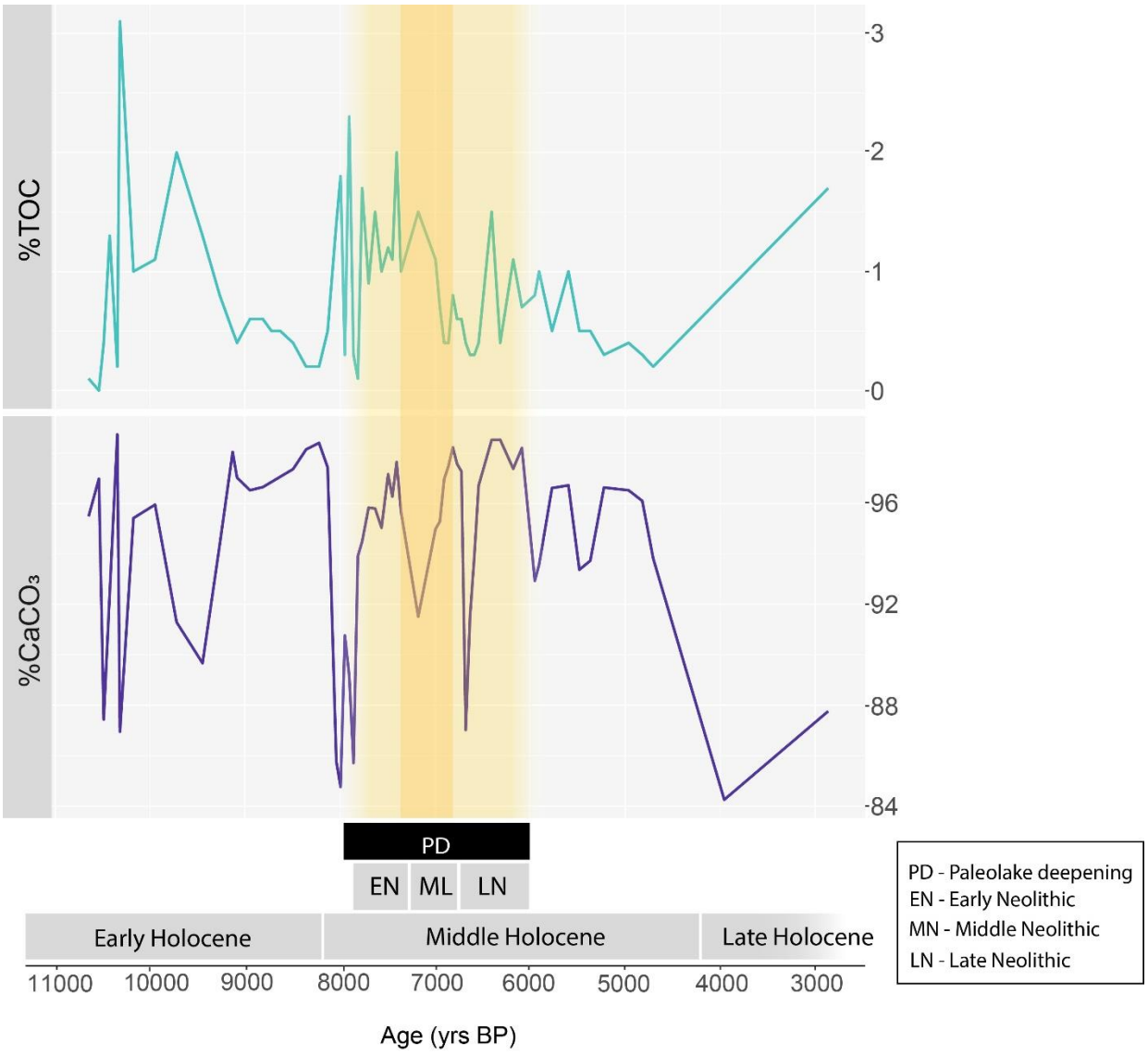

Figure 10. Geochemical profiles of %TOC and %$CaCO_3$ across the study interval with extreme (outlier) values removed. The dark yellow box indicates the Krivače habitation window, and the yellow shaded box indicates the window of surrounding habitation along the Dalmatia Coast. The interval of inferred paleolake deepening is indicated by the black box.

4.3.4 Pollen data

The largest pollen taxa contributors identified in the OSP-2 core include several varieties of Poaceae (grasses), Cyperaceae (sedges), *Betula* (birch), *Quercus* (oak), *Typha* (cattails). Smaller proportions of *Pinus* (pine), *Corylus* (hazel), *Juniperus* (juniper), *Fraxinus* (ash),

undifferentiated monocots, *Fern* (fern), *Nymphaceae* (lily), *Potamogeton* (pondweed), and flowering plant taxa including Asteraceae, Amaranthaceae, and *Euphorbia* were also observed. While it is difficult to establish trends in these vegetation types due to low sampling resolution and the limited age-range of samples, the occurrence of these taxa is consistent with the types of vegetation commonly found in the eastern Mediterranean and Adriatic during the Holocene.

This dataset is preliminary, and more pollen counts from this core or from other sites with better preservation potential in the Bribir-Ostrovica valley should be explored to fully understand how vegetation distributions may have changed in this location. Further descriptions of the OSP-2 pollen data and preliminary vegetation trends may be found in the appendix material.

5. Discussion

5.1 Data reliability and comparison with other Holocene paleoenvironmental records

The age-depth model produced for OSP-2 shows sample ages ranged from 10,647-2836 cal yrs BP. Agreement between these ages with radiocarbon dated artifacts from Krivače (McClure & Podrug, 2016; McClure, *under review*; Podrug *et al.*, *in press),* and preliminary pollen records that reflect regional the regional trend from mixed deciduous to scrubland vegetation suggest that radiocarbon ages are appropriately classified as Early to Late Holocene (Early to Late Neolithic).

Deep burial depths or evidence of local petroleum production can alter biomarker distributions and overprint primary vegetation and fire signals via catagenesis or petrogenesis. Given the shallow depth of the OSP-2 sediments, the lack of altered lithologies, and the absence of petroleum production sites within ~50 km of the study site (Fiket *et al.*, 2008), it is unlikely any secondary petrogenic processes occurred, and we currently interpret all biomarker

distributions as primary signatures. Radiocarbon dating of the even, short-chain *n*-alkanes could confirm fossil fuel sources did not contribute to this biomarker pool.

Trends amongst previous biogeochemical records for OSP-2 produced by others (%TOC, $\%CaCO_3$, $\delta^{13}C_{org}$, $\delta^{13}C_{carb}$, $\delta^{18}O$, pollen, and charcoal data) are complex and may reflect mixed sources. Most records appear to show weak or no relationship with Bond events.

%TOC and $\%CaCO_3$ inversely covary with one another. Of note are trends between 8000 and 6000 yrs BP. Here, %TOC values exceed 2 wt% and $\%CaCO_3$ values decrease by 13 wt%, both indicating a disturbance to the local environment. Increasing %TOC across the Krivače habitation interval coinciding with a decrease in $\%CaCO_3$ reflects greater organic matter and clastic sedimentation to the paleolake system. The gradual decrease in %TOC between ~7000–4700 yrs BP is not synchronous with $\%CaCO_3$ trends and may have been influenced by changing lake conditions that increased calcite precipitation.

$\delta^{13}C_{org}$ data do not vary with $\delta^{13}C_{carb}$ or %TOC and do not appear to reflect trends related to either climate or human activity. $\delta^{13}C_{carb}$ data demonstrate a gradual decreasing (negative) trend between the Early and Late Holocene that covaries with carbonate $\delta^{18}O$. The $\delta^{18}O$ record captures changes in both temperature and hydroclimate, which trend in opposite directions and could have overprinted one another in the recorded values. The long-term decreasing trend in $\delta^{18}O$ reported here is at odds with other Holocene $\delta^{18}O$ records in the Mediterranean, which show lake waters $\delta^{18}O$ values increased towards the modern (Eastwood *et al.*, 2006; Zielhofer *et al.*, 2018). The cause of the decreasing $\delta^{18}O$ record captured by OSP-2 is not known but may be tied to local shifts in lake water source, precipitation, evaporation, or a combination of these factors. Observations from Talbot (1990) and model results from Horton *et al.* (2016) suggest that fractionation driven primarily by evaporation during lake residence can

explain the covariation between $\delta^{18}O$ and $\delta^{13}C_{carb}$, which may explain why the $\delta^{18}O$ record captured by OSP-2 does not match other Holocene Mediterranean $\delta^{18}O$ records.

The OSP-2 pollen record is sparse, but the preliminary data align with pollen types found at other eastern Mediterranean and Adriatic sites, including multiple locations along the Dalmatia Coast (Lake Vrana, Malo Jerzo, and Busuja Bay; Di Rita & Magri, 2012; Lončar *et al.,* 2017; Kaniewski *et al.,* 2018). Grass pollen was present throughout the study interval and increased in abundance towards the Middle to Late Holocene boundary at 4200 yrs BP. Mixed deciduous (*Betula, Quercus, Corylus, Fern*) conifer (*Pinus*), aquatic (*Nymphaceae, Potamogeton*), and flowering plant pollen (*Asteraceae, Amaranthaceae, Euphorbia*) were detected through the Early and Middle Holocene. Conifer, aquatic, and flowering plant pollen counts decreased toward the Middle and Late Holocene boundary. Conversely, shrub (*Juniperus*) and sedge (*Cyperaceae*) pollen were not detected during the Early Holocene but appear near the Middle and Late Holocene. These trends reflect regional vegetation patterns, whereby mixed deciduous forests dominated the cool, wet Early Holocene and were gradually replaced by more resilient scrubland/shrub vegetation and higher proportions of grasses during the warmer, arid Middle and Late Holocene (Jalut *et al.,* 2009; Combourieu-Nebout *et al*., 2014). There is not sufficient evidence due to limited data resolution from the OSP-2 pollen record to evaluate vegetation changes as a function of human land usage, but the preliminary data are consistent with a gradual vegetation turnover in response to post-glacial warming.

Most data collected prior to biomarker analysis show evidence of climate-driven signals, whereas only one record (macrocharcoal) shows a distinct excursion across the Krivače habitation interval. Because of their coarse temporal resolution, more charcoal and pollen counts are required to determine if trends from these preliminary datasets persist through the OSP-2 core. Carbonate carbon and oxygen isotope records demonstrate synchronous behavior, which may be linked to the regional hydroclimate regime and enhanced evaporation. %TOC suggests elevated

contributions of organic material to the paleolake basin across the study interval, especially between ~8000–6000 yrs BP.

5.2 Biomarker distributions

N-alkane and PAH abundances increased sharply, and distribution ratios shifted strongly between the interval ~8000–6000 yrs BP. Podrug *et al.* (*in press*) indicate that the paleolake was relatively deep (with a maximum depth of 6 m) between ~8000–6000 yrs BP. Paleolake sediments from this interval include increased deposition of authigenic calcite precipitated from the water column, indicating a deeper lake environment relative to water levels during its residence time (Verrecchia, 2007; Podrug *et al.*, in press). Additionally, %TOC increased by 2.1 wt% between ~8000–6000 yrs BP, which may reflect paleolake deepening. Deeper basins allow for stabilized water columns, which enhance organic matter preservation, and thus could be responsible for elevated organic matter biomarker abundances. However, we cannot rule out the possibility that there may have been increased biomass flux to the basin from vegetation surrounding the paleolake in the Bribir-Ostrovica valley occurring simultaneously with lake deepening, whether by human or climate activity. One or both of these factors may have contributed to the larger abundances of *n*-alkanes and PAHs between ~8000–6000 yrs BP.

Human activity could explain the elevated biomarker distributions observed in OSP-2 by supplying additional weathered soils and/or nutrients to the paleolake basin. Radiocarbon dated artifacts from Krivače document the village was inhabited between ~7359–6950 yrs BP, although this time range is conservative (McClure & Podrug, 2016; McClure, *under review*; Podrug *et al.*, *in press*). The known period of habitation falls within the ~8000–6000 yrs BP interval defined by the biomarker profiles and is situated in the very middle of this range. If elevated biomarker distributions were a result of increased human activity, then this finding suggests habitation in the

lake catchment extended both prior to and following the currently accepted habitation period. This would have significant implications for understanding the habitation history at Krivače and at other nearby Neolithic sites in the Bribir-Ostrovica valley. Based on other case studies tying landscape disturbance and increased soil erosion to human activity (Hodell *et al.*, 1995; Simonneau *et al.*, 2013; Giguet-Covex *et al*., 2013), it is tempting to tie human influence on the biomarker distributions presented here. However, we also explore a climate-driven explanation for these results.

The ~8000–6000 yrs BP period defined by biomarker abundances was bracketed by Bond events at 8200 yrs BP and 5900 yrs BP that are correlated to drought conditions (dry winters) in the Mediterranean. These periods of increased aridity are observed at multiple sites in the eastern Mediterranean and Adriatic through oxygen isotope records and pollen records, which record changes in biomass to accommodate higher proportions of shrubs and scrublands (Di Rita & Magri, 2012). Depending on the morphology of the paleolake basin (open or closed) and the water inflow conditions, increasingly arid conditions may have reduced lake level (depth), lowered terrestrial and aquatic biomass production, and limited transport of terrestrial biomass by precipitation. These factors would collectively lead to lower *n*-alkane and PAH abundances. Evidence for relatively deeper paleolake conditions and higher abundances in *n*-alkane and PAH distributions do not agree with these expected results. However, precipitation extremes and associated flooding events could explain why the inferred lake depth was deeper than expected.

Benito *et al.* (2015a) and Benito *et al.* (2015b) report increased flooding activity in the eastern Mediterranean and Adriatic between ~8000–6500 yrs BP and a particularly intense flood period affecting lakes in this region between ~8000–7000 yrs BP based on alluvial horizons (Fig. 11; Benito *et al.*, 2015a; Benito *et al.*, 2015b). Local alluvial evidence recorded by McClure & Podrug (2016) support the occurrence of multiple flooding events during the habitation of Krivače (McClure & Podrug, 2016). Flooding is known to increase erosion, transport, and

redeposition of sediments in lake basins (Støren *et al.,* 2010), which would also increase transport and deposition of soil signatures. Given the coastal location of OSP-2 in the Bribir-Ostrovica valley, the open-basin paleolake conditions, and the available alluvial evidence, we suggest here that the increased depth of the paleolake between ~8000–6000 yrs BP may have been related to hydrologic extremes that led to increased flooding activity in the area, reflecting a climate-driven influence.

5.2.1 *N*-alkanes

N-alkanes show an unusual distribution through the study section. Prior to and following the ~8000–6000 yrs BP interval, distributions are dominated by typical odd long-chain homologs (C_{27}–C_{33}) indicative of contributions from terrestrial vegetation. Between ~8000–6000 yrs BP, even short-chain homologs (C_{16}–C_{22}) become nearly three times more abundant than the odd long-chain homologs, creating two modes of *n*-alkane distributions. There is a synchronous negative shift in ACL_{total} values, reflecting the dominance of short even-chain homologs.

In the introductory section, we discussed several mechanisms that can produce high abundances of even, short-chain *n*-alkanes including primary contributions from soils, biomass burning, contamination from fossil fuel hydrocarbons, and production by autochthonous bacteria. Kuhn *et al.* (2010) report even, short-chain homologs derived directly from woodland and grassland soil ranged from C_{14} to C_{20} with a maximum at C_{16}. Our even short-chain homologs range from C_{16} to C_{22} with a maximum at C_{18}. These results differ with those collected by Kuhn *et al.* (2010). It is possible smaller homologue *n*-alkanes were lost during sample handling when extracts or fractions were dried. Regardless, this hypothesis does not explain why even short-chain *n*-alkanes appear exclusively between ~8000–6000 yrs BP, but neither before nor after this

period. OSP-2 pollen counts do not support a major turnover in vegetation types across this interval, further weakening this production mechanism.

Biomass burning could potentially explain increased abundances of even, short-chain *n*-alkanes, especially given that the pyrogenic PAHs reported here also demonstrate peak abundances between ~8000–6000 yrs BP. Kuhn *et al.* (2010) report that burning can thermally break down long-chain *n*-alkanes to shorter-chain homologs. However, the pyrogenic PAH distribution normalized for biomass contributions against both C_{29} *n*-alkane and retene removed the enhanced pyrogenic signal. This indicates that the higher-than-average pyrogenic PAH abundances may reflect larger amounts of biomass available for burning, but it is unlikely that elevated flammability of biomass (Karp *et al.*, 2018) produced the unusual *n*-alkane distributions observed here.

Contamination from ancient hydrocarbon (i.e., fossil fuels or kerogen) sources can produce large proportions of even, short-chain *n*-alkanes. In some karst landscapes, it has been reported that hydrocarbons from deep fossil sources migrate upwards through the porous carbonate rock and mix with *n*-alkane pools in modern or recent sediments, creating allochthonous even short-chain distributions. Many Cretaceous-age source rocks and oil seeps have been identified along the Dalmatia Coast and in the Adriatic basin. However, there are no reports on oil seeps within ~50 km of Krivače that could contribute these short-chain *n*-alkanes (either even or odd) to the study site (Fiket *et al.*, 2008). Further, the distributions in OSP-2 do not match the even short-chain *n*-alkane distributions attributed to oil contamination by Kuhn *et al*. (C_{16}–C_{18}; 2010) nor distributions typical of crude oils (odd-dominated homologs C_{17}–C_{29}; Farrington & Meyer, 1975; Nishimura & Baker, 1986). Moreover, with the exception of one data point, CPI_{long} values also demonstrate values >1, indicating *n*-alkane contributions from biological sources and not secondary processes such as those recorded in fossil fuels (Bray & Evans, 1961). Hydrocarbon seeps are therefore an unlikely source.

Breakdown of plant waxes by microbes in the paleolake offers the strongest mechanism to explain these distributions. Microbial degradation of *n*-alkanes is reported to produce even distributions between C_{12} and $C_{22,}$ and in Wang *et al.* (2010), *n*-alkanes produced by lake bacteria ranged from C_{16} and C_{20} with a maximum at C_{18} (Elias *et al*., 1977; Ekpo *et al.*, 2005; Wang *et al.*, 2010). Unlike the other mechanisms that can produce even short-chain *n*-alkanes, the observations by Wang *et al.* (2010) align with the distribution of even, short-chain homologs in OSP-2. Wang *et al.* (2010) also noted a less-abundant grouping of odd, long-chain homologs occurring simultaneously with the highly abundant group of even, short-chain homologs (Wang *et al.*, 2010), similar to the *n*-alkanes distribution reported here. Further, CPI_{short} values are significantly greater between ~7800–6800 yrs BP, which support a biological source for these *n*-alkanes (Weisenberg *et al.*, 2009). If these *n*-alkanes are derived from microbial activity, then their higher abundances between ~8000–6000 yrs BP require an explanation related to changing environmental conditions that supported greater bacterial activity.

A deeper lake environment between ~8000–6000 yrs BP would allow for greater species richness, including microbes that could facilitate the breakdown of long odd-chain homologs (Hobæk *et al.*, 2002; Ekpo *et al.*, 2005; Wang *et al.*, 2010). The pAQ metric reaches its peak value at ~7000 yrs BP (though drops off before and after this maxima), indicating greater contributions from aquatic macrophytes during that time, but is a weak indicator of overall species richness. Regardless, it seems unlikely that deepening of the lake would singularly account for such productive microbial activity.

Human activity may have enhanced conditions in the lake that supported microbial communities in the paleolake. If more nutrients or fresh/fecal organic matter was supplied to the lake during this period, we would expect to see an increase in %TOC as a reflection of increased organic carbon inputs or productivity in the lake. Within the ~8000–6000 yrs BP interval, an elevated abundance pattern as other markers is clear for %TOC. This provides supporting

evidence of greater productivity associated with nutrient delivery, and/or greater preservation of organic inputs associated with paleolake deepening. Additionally, increased nutrient delivery can ramp phytoplankton growth, draw down available dissolved CO_2, and facilitate biogenic (authigenic) calcite precipitation, resulting in the loss of Ca^{2+} and alkalinity in the photic zone (Hamilton *et al.,* 2009). This further suggests that the *n*-alkane distributions were sourced by bacterial degradation in the paleolake that was possibly a result of nearby human activity.

5.2.2 PAHs

Pyrogenic PAHs and the PAH ratios explored here all show markedly distinct trends in their distributions between ~8000–6000 yrs BP. The key pyrogenic PAHs explored here (phenanthrene, fluoranthene, and pyrene) all show maximum values within this 2000-year period. Further, maximum pyrene and fluoranthene values occur at 7128 yrs BP, overlapping the habitation interval (7359–6950 yrs BP). Values produced by the retene/3-ring ratio and APDI between ~8000–7000 yrs BP also reach extreme values which, according to each index, suggest increased conifer burning. Thus, it is tempting to ascribe these abundance trends to human land-clearing practices.

We tested this by normalizing pyrene, the most abundant pyrogenic PAH, to vegetation biomass and specifically conifer biomass using the C_{29} *n*-alkane and the alkylated PAH retene, respectively. The normalization removed any significant trends, indicating that greater human burning activity was not the source of the PAH abundances. We originally hypothesized that PAHs should track the trends reflected in the *n*-alkane record if PAHs are responding to changes in local biomass composition rather than human activity, which is supported by the pyrogenic PAH distributions and the normalized pyrene distributions here. The fire compounds and biomass indicator compounds both increased in abundance simultaneously, suggesting their increases

were related to each other. We note that pyrogenic PAHs were elevated in abundance even though the total PAHs preserved did not shift between ~8000–6000 yrs BP. This indicates that greater proportions of pyrogenic PAHs during this interval are not an artifact of preservation.

Both elevated retene/3-ring ratios and decreased APDI values between ~8000–7000 yrs BP indicate increased conifer burning. Findings from Karp *et al.* (2020) showed that burning of conifers produces anomalous PAH distributions dominated by alkylated PAHs which can appear petrogenic, despite production from primary burning (Karp *et al.*, 2020). Enhanced abundances of alkylated PAHs could also be due to an increased contributions from soils, where PAHs distributions reflect some degree of organic weathering (Johnsen *et al.*, 2005; Zhang *et al.*, 2006; Karp *et al.*, 2021). Increased soil inputs could reflect greater flooding activity (Benito *et al.*, 2015a; Benito *et al.*, 2015), greater human landscape disturbance, or a combination of these. Therefore, these two metrics indicate increased conifer burning in concert with other biomass fires and greater soil inputs, both of which can lead to a greater proportion of alkylated PAHs.

5.3 Climate, human activity, and landscape change

Based on the lithological, geochemical, and biomarker evidence from this study and paleoclimate archives from the eastern Mediterranean and Adriatic, we explore two scenarios to explain the biomarker distributions explored here.

The first scenario invokes a climate-driven explanation. Climate change (temperature, hydroclimate) is cited as the principal driver of landscape change during the Holocene in the previous literature (Weiss & Bradley, 2001; Jalut *et al.*, 2009). Mediterranean paleoenvironmental archives strongly indicate extreme climate shifts resulting in multiple dry and wet phases (Fig. 11; Combourieu-Nebout *et al*., 2014; Lončar *et al.*, 2017). Hydroclimate dynamics in the Adriatic may have shifted during the ~8000-6000 yrs BP interval and increased

flooding activity along the Dalmatia Coast (Fig. 11). While exogenous sediment and oxygen isotope records do not demonstrate major changes to indicate flooding across this 2000-year interval, radiocarbon dated alluvium associated with multiple flood intervals at Krivače and other study sites in the Adriatic during this interval have been definitively identified (Støren *et al.*, 2010; Benito *et al.*, 2015a; Benito *et al.*, 2015b; McClure & Podrug, 2016). It may be that processes related to precipitation and evaporation dynamics, paleolake basin morphology, weathering, or other environmental factors overprinted flooding events.

Increased flooding would have 1) contributed to the temporary deepening of the paleolake, and 2) facilitated greater surface transport of biomass to the basin. Cumulatively, these processes could explain the significant abundance of both *n*-alkanes and PAHs across this interval. Normalized PAHs tracked a lipid biomass proxy, consistent with the strong covariance between amplified *n*-alkane and PAH distributions.

The predominance of short even-chain *n*-alkanes between ~8000–6000 yrs BP is unusual but could be explained by preservation biases if climate was the sole driver (Fig. 11). Based on the production mechanisms of even, short-chain homologs reviewed in this text and comparison to the geochemical and PAH data, bacterial production appears to be the most likely source of these *n*-alkanes. This process could have occurred before and after ~8000–6000 yrs BP but may not appear in these records due to degradation or overprinting in a shallower paleolake setting.

Alternatively, we propose a combined climate-human activity scenario to explain observed biomarker distributions. Archaeological and geochemical evidence from Krivače and other contemporaneous human habitation sites in the Bribir-Ostrovica valley from the Early to Late Neolithic demonstrate the progressive construction of permanent settlement structures and the implementation of early agricultural practices and animal husbandry (Fig. 11). If farming activities were employed (vegetation cutting, burning, manuring, crop cultivation) at Krivače, their signatures may be entangled in or overprinted by climate-driven shifts in the geochemical

records and the biomarker distributions presented here. Therefore, it may be that climate drove paleolake deepening between ~8000–6000 yrs BP in the same manner as described above (hydroclimate variability and frequent flooding), but that increased land-usage simultaneously exported larger proportions of biomass and nutrients to the basin, resulting in the elevated *n*-alkane distributions observed during this period (Hodell *et al.,* 1995; Weiss & Bradley, 2001; Simonneau *et al.*, 2013; Giguet-Covex *et al*., 2013).

A combination of nutrients and greater surface transport could have easily amplified microbial productivity to produce the high proportions of even, short-chain *n*-alkanes here. Amplified PAH abundances occur through this same interval, even after normalizing pyrogenic PAHs to total PAHS, which could also reflect an increase in nearby landscape disturbance. These OSP-2 biomarker distributions may not be simple reflections of Adriatic climate, but indicators of major human activity at Krivače between ~8000–6000 yrs BP.

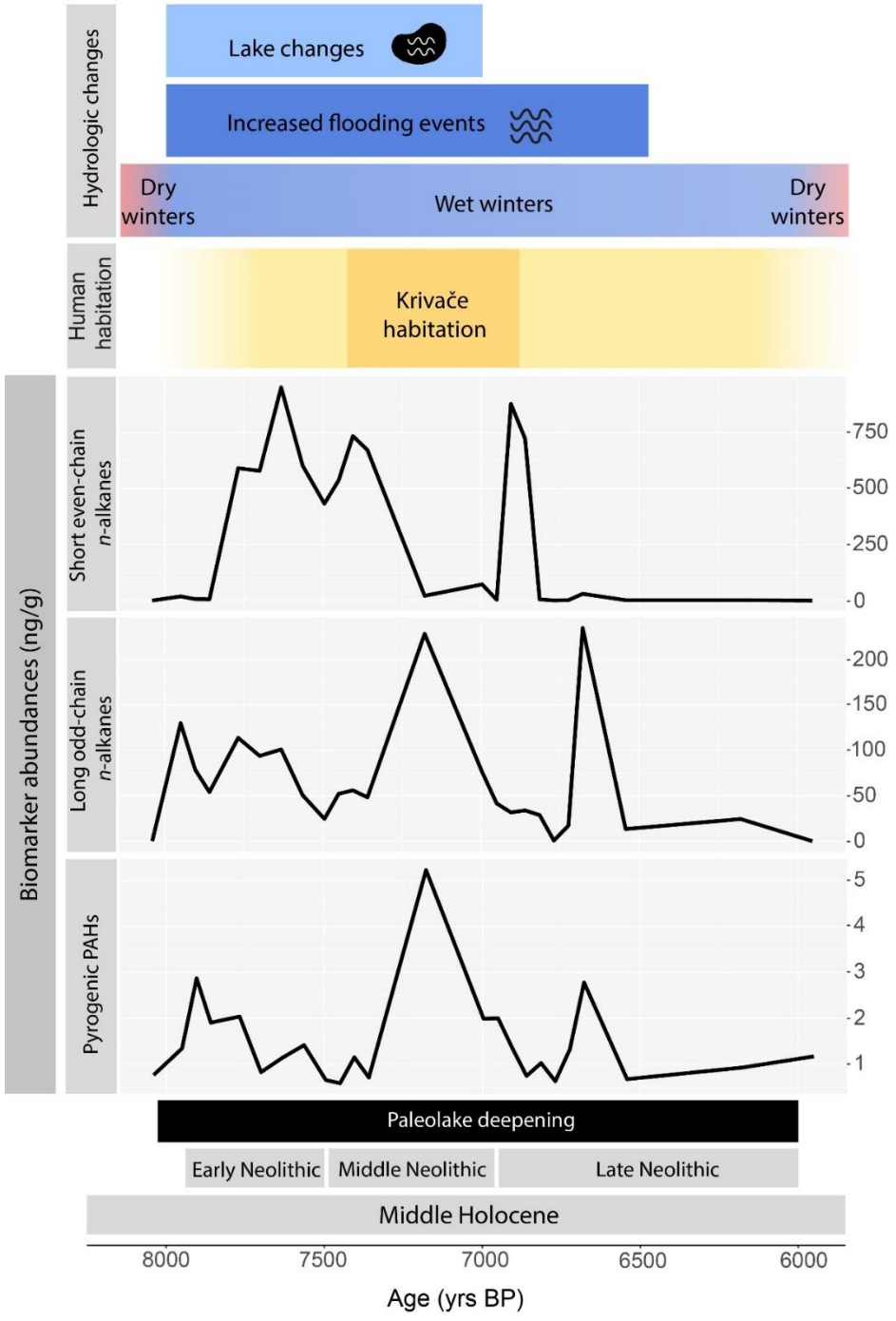

Figure 11. Summary figure of hydrologic changes (lake changes, flooding events, and wet and dry winter periods linked to Bond events), human habitation, and averaged biomarker distributions (ng/g) of even, short-chain n-alkanes, odd, long-chain n-alkanes, and pyrogenic PAHs between 8000 and 6000 BP. The dark yellow box indicates the Krivače habitation window, and the yellow shaded box indicates the window of surrounding habitation along the Dalmatia Coast. The interval of inferred paleolake deepening is indicated by the black box.

5.4 Future directions

The findings presented here raise many questions about the relationships between human activity, climate, and their effect(s) on landscape changes in the Bribir-Ostrovica valley during the Holocene. We proposed two scenarios that could explain the biomarker distributions observed in OSP-2, with special attention to the predominant even, short-chain *n*-alkanes present between ~8000–6000 yrs BP. Collection of additional geochemical proxies could help distinguish whether human activity has a marked influence on these biomarker distributions, or if they are a primary reflection of climate change in the eastern Mediterranean.

A fecal sterol distribution would help inform the degree of human activity at Krivače. Fecal sterols mainly consist of 5β-stanols and are produced during digestion (Harrault *et al.,* 2019). Different mammals have characteristic stanol distribution patterns that can be diagnostic for animal-sourced fecal matter inputs (Harrault *et al.,* 2019). Higher proportions of fecal sterols, especially those from domesticates (cows, sheep, or goats), would provide supporting evidence for increasing animal husbandry or manuring practices. Either of these activities could supply increased amounts of organic matter and nutrients to the paleolake basin, thus contributing to the eutrophication of the paleolake by increasing microbial primary productivity and producing even, short-chain *n*-alkane distributions (Wang *et al.,* 2010).

Biomarkers specific to microbes may be a key area of future research to further assess the potential role of enhanced microbial activity between ~8000–6000 yrs BP. For example, hopanoids synthesized by anaerobic microbes have recently been identified in anoxic methane-oxidizing environments (Fischer *et al.,* 2005). A combined record showing increased abundances of fecal sterol and hopanoid biomarkers would provide a compelling argument for microbial production of even, short-chain *n*-alkanes facilitated by nutrient loading from amplified human activity at Krivače.

Additional biomarker and isotope records could inform on temperature and hydroclimate trends in the local environment. For example, branched and archaeal glycerol dialkyl glycerol tetraethers (GDGTs) are increasingly used as temperature proxies in sedimentary archives and have recently been proposed as a proxy for paleolake level (Zink *et al.*, 2010; Wang *et al.*, 2014). GDGTs are ubiquitous isoprenoid compounds produced either by archaea or bacteria, which create branched varieties (Zink *et al.*, 2010). GDGTs record temperature changes from the surrounding environment in the membranes of their producing organism, which become preserved when the organism dies and is buried in the sediment (Zink *et al.*, 2010; Loomis *et al.*, 2012). Temperature records can be extracted from GDGT compounds using methods such as the TEX_{86} index to reconstruct paleoenvironmental changes to the local environment (Zink *et al.*, 2010; Loomis *et al.*, 2012). Simultaneously, Wang *et al.* (2014) found that the proportion of the archaeal GDGT thaumarchaeol to the total amount of archaeal GDGTs in sediments increases significantly with water depth (Wang *et al.*, 2010). A GDGT record for OSP-2 would provide more concrete evidence of local temperature and lake level (i.e., hydroclimate) changes. The latter could be used to normalize biomarker contributions against changing depth in the paleolake, which would clarify changes in water depth and thus, preservation potential.

Hydrogen isotopes (D/H, or δD) from plant waxes can be used to reconstruct changes to local hydroclimate by tracking the enrichment or depletion of δD relative to changes in temperature. Hydrogen isotopes due to their low molecular mass tend to fractionate strongly due to either equilibrium or kinetic isotope effects (Sessions, 2016). Their high sensitivity is useful for tracking minute local evaporation and precipitation trends but can also lead to extreme variations in environmental waters (Sessions, 2016). Thus, additional temperature and paleoenvironmental records are essential for interpreting δD results. A combined GDGT and δD record from OSP-2 would create a cohesive picture of temperature and hydroclimate change affecting the Bribir-

Ostrovica valley during the Holocene and clarify the driver of paleolake deepening between ~8000–6000 yrs BP.

6. Conclusions

The biomarker data from the OSP-2 core reveal several important findings regarding human and climate influences on landscape changes during the Holocene and may possibly have important implications for habitation history at Krivače. Trends in %TOC, $\%CaCO_3$, $\delta^{13}C_{org}$, $\delta^{13}C_{carb}$, $\delta^{18}O$, and preliminary charcoal and pollen data may reflect mixed sources between changing Mediterranean climate dynamics and human activity. Of note are excursions in %TOC, and trends in charcoal and pollen records that suggest changing environmental conditions across the ~8000–6000 yrs BP window. A major change in local conditions is likewise recorded by coeval increases in *n*-alkane and PAH abundances between ~8000–6000 yrs BP.

At minimum, we suggest these distributions are a product of increased flooding driven by local hydroclimate changes, which deepened the paleolake and aided in surface transport of biomass. At maximum, nearby human activity at Krivače may have amplified these distributions by contributing excess nutrients to the watershed. The predominant even, short-chain *n*-alkane and PAH distributions preserved between ~8000–6000 yrs BP do not align with expected distributions/conditions ascribed to contributions from primary vegetation, fossil hydrocarbons, or biomass burning. Therefore, we suspect *n*-alkane patterns are a result of autochthonous bacterial production in the paleolake and PAHs reflect soil disturbance and transport, which may or may not have been tied to human activity. Future research endeavors should focus on understanding the environmental conditions, bacterial types, and enzymatic pathways responsible for *n*-alkane production in lacustrine settings and signatures of soil inputs to better contextualize these results.

This study lends support to interpretations of pervasive climate influence on paleoenvironmental signals captured in sedimentary archives during the Holocene. If the distributions described here are simultaneously a product of human activity, then it is likely that Krivače was inhabited from greater lengths than between 7359–6950 yrs BP. By virtue, this would also constrain the onset and regional spread of agricultural practices in this region that was a gateway connecting Europe to the Neolithic Revolution in the Mediterranean and Middle East.

References

Benito, G., Macklin, M. G., Panin, A., Rossato, S., Fontana, A., Jones, A. F., Machado, M. J., Matlakhova, E., Mozzi, P., & Zielhofer, C. (2015). Recurring flood distribution patterns related to short-term Holocene climatic variability. In Scientific Reports (Vol. 5, Issue 1). Springer Science and Business Media LLC. https://doi.org/10.1038/srep16398

Benito, G., Macklin, M. G., Zielhofer, C., Jones, A. F., & Machado, M. J. (2015). Holocene flooding and climate change in the Mediterranean. In CATENA (Vol. 130, pp. 13–33). Elsevier BV. https://doi.org/10.1016/j.catena.2014.11.014

Berger, J.-F., Lespez, L., Kuzucuoğlu, C., Glais, A., Hourani, F., Barra, A., & Guilaine, J. (2016). Interactions between climate change and human activities during the early to mid-Holocene in the eastern Mediterranean basins. In Climate of the Past (Vol. 12, Issue 9, pp. 1847–1877). Copernicus GmbH. https://doi.org/10.5194/cp-12-1847-2016

Blumer, M., & Youngblood, W. W. (1975). Polycyclic Aromatic Hydrocarbons in Soils and Recent Sediments. In Science (Vol. 188, Issue 4183, pp. 53–55). American Association for the Advancement of Science (AAAS). https://doi.org/10.1126/science.188.4183.53

Bond, G., Showers, W., Cheseby, M., Lotti, R., Almasi, P., deMenocal, P., Priore, P., Cullen, H., Hajdas, I., & Bonani, G. (1997). A Pervasive Millennial-Scale Cycle in North Atlantic Holocene and Glacial Climates. In Science (Vol. 278, Issue 5341, pp. 1257–1266). American Association for the Advancement of Science (AAAS). https://doi.org/10.1126/science.278.5341.1257

Bond, G., Kromer, B., Beer, J., Muscheler, R., Evans, M. N., Showers, W., Hoffmann, S., Lotti-Bond, R., Hajdas, I., & Bonani, G. (2001). Persistent Solar Influence on North Atlantic Climate During the Holocene. In Science (Vol. 294, Issue 5549, pp. 2130–2136). American Association for the Advancement of Science (AAAS). https://doi.org/10.1126/science.1065680

Bray, E. E., & Evans, E. D. (1961). Distribution of n-paraffins as a clue to recognition of source beds. In Geochimica et Cosmochimica Acta (Vol. 22, Issue 1, pp. 2–15). Elsevier BV. https://doi.org/10.1016/0016-7037(61)90069-2

Callaghan, A. V., Wawrik, B., Ní Chadhain, S. M., Young, L. Y., & Zylstra, G. J. (2008). Anaerobic alkane-degrading strain AK-01 contains two alkylsuccinate synthase genes. In Biochemical and Biophysical Research Communications (Vol. 366, Issue 1, pp. 142–148). Elsevier BV. https://doi.org/10.1016/j.bbrc.2007.11.094

Carvajal-Ortiz, H., & Gentzis, T. (2015). Critical considerations when assessing hydrocarbon plays using Rock-Eval pyrolysis and organic petrology data: Data quality revisited. In International Journal of Coal Geology (Vol. 152, pp. 113–122). Elsevier BV. https://doi.org/10.1016/j.coal.2015.06.001

Combourieu-Nebout, N., Peyron, O., Bout-Roumazeilles, V., Goring, S., Dormoy, I., Joannin, S., Sadori, L., Siani, G., & Magny, M. (2013). Holocene vegetation and climate changes in the central Mediterranean inferred from a high-resolution marine pollen record (Adriatic Sea). In Climate of the Past (Vol. 9, Issue 5, pp. 2023–2042). Copernicus GmbH. https://doi.org/10.5194/cp-9-2023-2013

Conte, M., Giuffrida, A., & Tedesco, S. (1989). Mediterranean Oscillation: Impact on Precipitation and Hydrology in Italy. In Conference on Climate and Water. (Vol. 1).

Cravo-Laureau, C., Grossi, V., Raphel, D., Matheron, R., & Hirschler-Réa, A. (2005). Anaerobic n -Alkane Metabolism by a Sulfate-Reducing Bacterium, Desulfatibacillum aliphaticivorans Strain CV2803 T. In Applied and Environmental Microbiology (Vol. 71, Issue 7, pp. 3458–3467). American Society for Microbiology. https://doi.org/10.1128/aem.71.7.3458-3467.2005

Denis, E. H., Toney, J. L., Tarozo, R., Scott Anderson, R., Roach, L. D., & Huang, Y. (2012). Polycyclic aromatic hydrocarbons (PAHs) in lake sediments record historic fire events: Validation using HPLC-fluorescence detection. In Organic Geochemistry (Vol. 45, pp. 7–17). Elsevier BV. https://doi.org/10.1016/j.orggeochem.2012.01.005

Denis, E. H., Maibauer, B. J., Bowen, G. J., Jardine, P. E., Harrington, G. J., Baczynski, A. A., McInerney, F. A., Collinson, M. E., Belcher, C. M., Wing, S. L., & Freeman, K. H. (2021). Decreased soil carbon in a warming world: Degraded pyrogenic carbon during the Paleocene-Eocene Thermal Maximum, Bighorn Basin, Wyoming. In Earth and Planetary Science Letters (Vol. 566, p. 116970). Elsevier BV. https://doi.org/10.1016/j.epsl.2021.116970

Dettweiler, C., Knicker, H., González-Vila, F. J., Almendros Martín, G., & Zancada Fernández, M. C. (2003). Monitoring the fire impacts on soil through chromatographic analysis of the lipid fraction.

Di Rita, F., & Magri, D. (2012). An overview of the Holocene vegetation history from the central Mediterranean coasts [JB]. 4, 35–52. https://doi.org/10.3304/JMES.2012.003

Diefendorf, A. F., Freeman, K. H., & Wing, S. L. (2014). A comparison of terpenoid and leaf fossil vegetation proxies in Paleocene and Eocene Bighorn Basin sediments. In Organic Geochemistry (Vol. 71, pp. 30–42). Elsevier BV. https://doi.org/10.1016/j.orggeochem.2014.04.004

Diefendorf, A. F., & Freimuth, E. J. (2017). Extracting the most from terrestrial plant-derived n-alkyl lipids and their carbon isotopes from the sedimentary record: A review. In Organic Geochemistry (Vol. 103, pp. 1–21). Elsevier BV. https://doi.org/10.1016/j.orggeochem.2016.10.016

Eastwood, W. J., Leng, M. J., Roberts, N., & Davis, B. (2007). Holocene climate change in the eastern Mediterranean region: a comparison of stable isotope and pollen data from Lake Gölhisar, southwest Turkey. In Journal of Quaternary Science (Vol. 22, Issue 4, pp. 327–341). Wiley. https://doi.org/10.1002/jqs.1062

Eckmeier, E., & Wiesenberg, G. L. B. (2009). Short-chain n-alkanes (C16–20) in ancient soil are useful molecular markers for prehistoric biomass burning. In Journal of Archaeological Science (Vol. 36, Issue 7, pp. 1590–1596). Elsevier BV. https://doi.org/10.1016/j.jas.2009.03.021

Eglinton, G., & Hamilton, R. J. (1967). Leaf Epicuticular Waxes. In Science (Vol. 156, Issue 3780, pp. 1322–1335). American Association for the Advancement of Science (AAAS). https://doi.org/10.1126/science.156.3780.1322

Eglinton, G., Gonzalez, A. G., Hamilton, R. J., & Raphael, R. A. (1962). Hydrocarbon constituents of the wax coatings of plant leaves: A taxonomic survey. In Phytochemistry (Vol. 1, Issue 2, pp. 89–102). Elsevier BV. https://doi.org/10.1016/s0031-9422(00)88006-1

Ekpo, B. O., Oyo-Ita, O. E., & Wehner, H. (2005). Even-n-alkane/alkene predominances in surface sediments from the Calabar River, SE Niger Delta, Nigeria. In Naturwissenschaften (Vol. 92, Issue 7, pp. 341–346). Springer Science and Business Media LLC. https://doi.org/10.1007/s00114-005-0639-8

Elias, V. O., Simoneit, B. R. T., & Cardoso, J. N. (1997). Even N-Alkane Predominances on the Amazon Shelf and A Northeast Pacific Hydrothermal System. In Naturwissenschaften (Vol. 84, Issue 9, pp. 415–420). Springer Science and Business Media LLC. https://doi.org/10.1007/s001140050421

Escobar, M., Márquez, G., Inciarte, S., Rojas, J., Esteves, I., & Malandrino, G. (2011). The organic geochemistry of oil seeps from the Sierra de Perijá eastern foothills, Lake Maracaibo Basin, Venezuela. In Organic Geochemistry (Vol. 42, Issue 7, pp. 727–738). Elsevier BV. https://doi.org/10.1016/j.orggeochem.2011.06.005

Farrington, J. W., & Meyer, P. A. (1975). Hydrocarbons in the marine environment. In Environmental Chemistry (pp. 109–136). Royal Society of Chemistry. https://doi.org/10.1039/9781847555984-00109

Ficken, K. J., Li, B., Swain, D. L., & Eglinton, G. (2000). An n-alkane proxy for the sedimentary input of submerged/floating freshwater aquatic macrophytes. In Organic Geochemistry (Vol. 31, Issues 7–8, pp. 745–749). Elsevier BV. https://doi.org/10.1016/s0146-6380(00)00081-4

Fiket, Ž., Alajbeg, A., Strmić Palinkaš, S., Tari-Kovačić, V., Palinkaš, L., & Spangenberg, J. (2008). Organic geochemistry of Jurassic-Cretaceous source rocks and oil seeps from the profile across the Adriatic-Dinaric carbonate platform.

Fischer, W. W., Summons, R. E., & Pearson, A. (2005). Targeted genomic detection of biosynthetic pathways: anaerobic production of hopanoid biomarkers by a common sedimentary microbe. In Geobiology (Vol. 3, Issue 1, pp. 33–40). Wiley. https://doi.org/10.1111/j.1472-4669.2005.00041.x

Forenbaher, S., & Miracle, P. T. (2005). The spread of farming in the Eastern Adriatic. In Antiquity (Vol. 79, Issue 305, pp. 514–528). Cambridge University Press (CUP). https://doi.org/10.1017/s0003598x00114474

Freeman, K. H., & Pancost, R. D. (2014). Biomarkers for Terrestrial Plants and Climate. In Treatise on Geochemistry (pp. 395–416). Elsevier. https://doi.org/10.1016/b978-0-08-095975-7.01028-7

Gagnon, C. (2021). Hydrologic and Landscape Evolution Near a Neolithic Settlement in Dalmatia, Croatia. [Unpublished undergraduate thesis]. The Pennsylvania State University.

Gajic-Capka, M., & Zaninovic, K. (2006). Long-term trends in temperature, precipitation and runoff at the Croatian Eastern Adriatic Coast. *Proc. Balwois, Ohrid*, *23*(26.5), 2006.

Giguet-Covex, C., Pansu, J., Arnaud, F., Rey, P.-J., Griggo, C., Gielly, L., Domaizon, I., Coissac, E., David, F., Choler, P., Poulenard, J., & Taberlet, P. (2014). Long livestock farming history and human landscape shaping revealed by lake sediment DNA. In Nature Communications (Vol. 5, Issue 1). Springer Science and Business Media LLC. https://doi.org/10.1038/ncomms4211

Goodess, C. M., & Jones, P. D. (2002). Links between circulation and changes in the characteristics of Iberian rainfall. In International Journal of Climatology (Vol. 22, Issue 13, pp. 1593–1615). Wiley. https://doi.org/10.1002/joc.810

Hamilton, S. K., Bruesewitz, D. A., Horst, G. P., Weed, D. B., & Sarnelle, O. (2009). Biogenic calcite–phosphorus precipitation as a negative feedback to lake eutrophication. In Canadian Journal of Fisheries and Aquatic Sciences (Vol. 66, Issue 2, pp. 343–350). Canadian Science Publishing. https://doi.org/10.1139/f09-003

Harrault, L., Milek, K., Jardé, E., Jeanneau, L., Derrien, M., & Anderson, D. G. (2019). Faecal biomarkers can distinguish specific mammalian species in modern and past environments. In J. J. Loor (Ed.), PLOS ONE (Vol. 14, Issue 2, p. e0211119). Public Library of Science (PLoS). https://doi.org/10.1371/journal.pone.0211119

Hobæk, A., Manca, M., & Andersen, T. (2002). Factors influencing species richness in lacustrine zooplankton. In Acta Oecologica (Vol. 23, Issue 3, pp. 155–163). Elsevier BV. https://doi.org/10.1016/s1146-609x(02)01147-5

Hodell, D. A., Curtis, J. H., & Brenner, M. (1995). Possible role of climate in the collapse of Classic Maya civilization. In Nature (Vol. 375, Issue 6530, pp. 391–394). Springer Science and Business Media LLC. https://doi.org/10.1038/375391a0

Horton, T. W., Defliese, W. F., Tripati, A. K., & Oze, C. (2016). Evaporation induced 18O and 13C enrichment in lake systems: A global perspective on hydrologic balance effects. In Quaternary Science Reviews (Vol. 131, pp. 365–379). Elsevier BV. https://doi.org/10.1016/j.quascirev.2015.06.030

Hurrell, J. W., Kushnir, Y., Ottersen, G., & Visbeck, M. (2003). An overview of the North Atlantic Oscillation. In The North Atlantic Oscillation: Climatic Significance and Environmental Impact (pp. 1–35). American Geophysical Union. https://doi.org/10.1029/134gm01

Ilijanić, N., Miko, S., Hasan, O., & Bakrač, K. (2018). Holocene environmental record from lake sediments in the Bokanjačko blato karst polje (Dalmatia, Croatia). In Quaternary International (Vol. 494, pp. 66–79). Elsevier BV. https://doi.org/10.1016/j.quaint.2018.01.037

Jalut, G., Dedoubat, J. J., Fontugne, M., & Otto, T. (2009). Holocene circum-Mediterranean vegetation changes: Climate forcing and human impact. In Quaternary International (Vol. 200, Issues 1–2, pp. 4–18). Elsevier BV. https://doi.org/10.1016/j.quaint.2008.03.012

Jansen, B., Haussmann, N. S., Tonneijck, F. H., Verstraten, J. M., & de Voogt, P. (2008). Characteristic straight-chain lipid ratios as a quick method to assess past forest–páramo transitions in the

Ecuadorian Andes. In Palaeogeography, Palaeoclimatology, Palaeoecology (Vol. 262, Issues 3–4, pp. 129–139). Elsevier BV. https://doi.org/10.1016/j.palaeo.2008.02.007

Jetter, R., & Kunst, L. (2008). Plant surface lipid biosynthetic pathways and their utility for metabolic engineering of waxes and hydrocarbon biofuels. In The Plant Journal (Vol. 54, Issue 4, pp. 670–683). Wiley. https://doi.org/10.1111/j.1365-313x.2008.03467.x

Johnsen, A. R., Wick, L. Y., & Harms, H. (2005). Principles of microbial PAH-degradation in soil. In Environmental Pollution (Vol. 133, Issue 1, pp. 71–84). Elsevier BV. https://doi.org/10.1016/j.envpol.2004.04.015

Jones, M. D., & Neil Roberts, C. (2008). Interpreting lake isotope records of Holocene environmental change in the Eastern Mediterranean. In Quaternary International (Vol. 181, Issue 1, pp. 32–38). Elsevier BV. https://doi.org/10.1016/j.quaint.2007.01.012

Kaniewski, D., Marriner, N., Morhange, C., Rius, D., Carre, M.-B., Faivre, S., & Van Campo, E. (2018). Croatia's mid-Late Holocene (5200-3200 BP) coastal vegetation shaped by human societies. In Quaternary Science Reviews (Vol. 200, pp. 334–350). Elsevier BV. https://doi.org/10.1016/j.quascirev.2018.10.004

Kappenberg, A., Braun, M., Amelung, W., & Lehndorff, E. (2019). Fire condensates and charcoals: Chemical composition and fuel source identification. In Organic Geochemistry (Vol. 130, pp. 43–50). Elsevier BV. https://doi.org/10.1016/j.orggeochem.2019.01.009

Karp, A. T., Behrensmeyer, A. K., & Freeman, K. H. (2018). Grassland fire ecology has roots in the late Miocene. In Proceedings of the National Academy of Sciences (Vol. 115, Issue 48, pp. 12130–12135). Proceedings of the National Academy of Sciences. https://doi.org/10.1073/pnas.1809758115

Karp, A. T., Holman, A. I., Hopper, P., Grice, K., & Freeman, K. H. (2020). Fire distinguishers: Refined interpretations of polycyclic aromatic hydrocarbons for paleo-applications. In Geochimica et

Cosmochimica Acta (Vol. 289, pp. 93–113). Elsevier BV. https://doi.org/10.1016/j.gca.2020.08.024

Karp, A. T., Andrae, J. W., McInerney, F. A., Polissar, P. J., & Freeman, K. H. (2021). Soil Carbon Loss and Weak Fire Feedbacks During Pliocene C 4 Grassland Expansion in Australia. In Geophysical Research Letters (Vol. 48, Issue 2). American Geophysical Union (AGU). https://doi.org/10.1029/2020gl090964

Köppen, W. (1923). Die Klimate der Erde. De Gruyter. https://doi.org/10.1515/9783111491530

Kuhn, T. K., Krull, E. S., Bowater, A., Grice, K., & Gleixner, G. (2010). The occurrence of short chain n-alkanes with an even over odd predominance in higher plants and soils. In Organic Geochemistry (Vol. 41, Issue 2, pp. 88–95). Elsevier BV. https://doi.org/10.1016/j.orggeochem.2009.08.003

Laflamme, R. E., & Hites, R. A. (1978). The global distribution of polycyclic aromatic hydrocarbons in recent sediments. In Geochimica et Cosmochimica Acta (Vol. 42, Issue 3, pp. 289–303). Elsevier BV. https://doi.org/10.1016/0016-7037(78)90182-5

Lichtfouse, É., Bardoux, G., Mariotti, A., Balesdent, J., Ballentine, D. C., & Macko, S. A. (1997). Molecular, 13C, and 14C evidence for the allochthonous and ancient origin of C16C18 n-alkanes in modern soils. In Geochimica et Cosmochimica Acta (Vol. 61, Issue 9, pp. 1891–1898). Elsevier BV. https://doi.org/10.1016/s0016-7037(97)00021-5

Liu, W., Yang, H., Wang, H., Yao, Y., Wang, Z., & Cao, Y. (2016). Influence of aquatic plants on the hydrogen isotope composition of sedimentary long-chain n-alkanes in the Lake Qinghai region, Qinghai-Tibet Plateau. In Science China Earth Sciences (Vol. 59, Issue 7, pp. 1368–1377). Springer Science and Business Media LLC. https://doi.org/10.1007/s11430-016-5263-2

Liu, J., An, Z., & Liu, H. (2018). Leaf wax n-alkane distributions across plant types in the central Chinese Loess Plateau. In Organic Geochemistry (Vol. 125, pp. 260–269). Elsevier BV. https://doi.org/10.1016/j.orggeochem.2018.09.006

Lončar, N., Bar-Matthews, M., Avalon, A., Surić, M., & Faivre, S. (2017). Early and mid-holocene environmental conditions in the eastern Adriatic recorded in speleothems from Mala Špilja cave and Velika Špilja cave (Mljet island, Croatia). In Acta Carsologica (Vol. 46, Issues 2–3). The Research Center of the Slovenian Academy of Sciences and Arts / Znanstvenoraziskovalni center Slovenske akademije znanosti in umetnosti (ZRC SAZU). https://doi.org/10.3986/ac.v46i2-3.4939

Loomis, S. E., Russell, J. M., Ladd, B., Street-Perrott, F. A., & Sinninghe Damsté, J. S. (2012). Calibration and application of the branched GDGT temperature proxy on East African lake sediments. In Earth and Planetary Science Letters (Vols. 357–358, pp. 277–288). Elsevier BV. https://doi.org/10.1016/j.epsl.2012.09.031

López-Avilés, A., García-Alix, A., Jiménez-Moreno, G., Anderson, R. S., Toney, J. L., Mesa-Fernández, J. M., & Jiménez-Espejo, F. J. (2021). Latest Holocene paleoenvironmental and paleoclimate reconstruction from an alpine bog in the Western Mediterranean region: The Borreguil de los Lavaderos de la Reina record (Sierra Nevada). In Palaeogeography, Palaeoclimatology, Palaeoecology (Vol. 573, p. 110434). Elsevier BV. https://doi.org/10.1016/j.palaeo.2021.110434

Lyons, S. L., Karp, A. T., Bralower, T. J., Grice, K., Schaefer, B., Gulick, S. P. S., Morgan, J. V., & Freeman, K. H. (2020). Organic matter from the Chicxulub crater exacerbated the K–Pg impact winter. In Proceedings of the National Academy of Sciences (Vol. 117, Issue 41, pp. 25327–25334). Proceedings of the National Academy of Sciences. https://doi.org/10.1073/pnas.2004596117

Magill, C. R., Denis, E. H., & Freeman, K. H. (2015). Rapid sequential separation of sedimentary lipid biomarkers via selective accelerated solvent extraction. In Organic Geochemistry (Vol. 88, pp. 29–34). Elsevier BV. https://doi.org/10.1016/j.orggeochem.2015.07.009

Martin-Vide, J., & Lopez-Bustins, J.-A. (2006). The Western Mediterranean Oscillation and rainfall in the Iberian Peninsula. In International Journal of Climatology (Vol. 26, Issue 11, pp. 1455–1475). Wiley. https://doi.org/10.1002/joc.1388

McClure, S.B., The Balkan Coastal Neolithic – The Adriatic Coast. In: Galaty, M., Parkinson, W., Gyucha, A. (eds), *Oxford Handbook of Balkan Prehistory*. Oxford. Under review.

McClure, S.B., Podrug, E. Ebert, C.E., Buckley, G.M., Jović, J., Moore, A.M.T., Triozzi, N., Welker, M.H., Zavodny, E., Krigbaum, J., Freeman, K.H., Kennett, D.J. In prep. Isotopic evidence for intensified dairying and transhumance in the Adriatic. To be submitted to *PLoSOne* (est. submission June 2022) McClure, S. B., & Podrug, E. (2016). Fresh Fields and Pastures New: Papers Presented in Honor of Andrew MT Moore.

McClure, S. B., Magill, C., Podrug, E., Moore, A. M. T., Harper, T. K., Culleton, B. J., Kennett, D. J., & Freeman, K. H. (2018). Fatty acid specific δ13C values reveal earliest Mediterranean cheese production 7,200 years ago. In J. J. Loor (Ed.), PLOS ONE (Vol. 13, Issue 9, p. e0202807). Public Library of Science (PLoS). https://doi.org/10.1371/journal.pone.0202807

Miller, D. R., Castañeda, I. S., Bradley, R. S., & MacDonald, D. (2017). Local and regional wildfire activity in central Maine (USA) during the past 900 years. In Journal of Paleolimnology (Vol. 58, Issue 4, pp. 455–466). Springer Science and Business Media LLC. https://doi.org/10.1007/s10933-017-0002-z

Nioti, D. & Maravelis, Angelos & Tserolas, Panos & Zelilidis, Avraam. (2017). TOC and CaCO3 content in Oligocene shelf deposits on Lemnos Island and their relation with depositional conditions. Bulletin of the Geological Society of Greece. 47. 852. 10.12681/bgsg.11124.

Nishimura, M., & Baker, E. W. (1986). Possible origin of with a remarkable even-to-odd predominance in recent marine sediments. In Geochimica et Cosmochimica Acta (Vol. 50, Issue 2, pp. 299–305). Elsevier BV. https://doi.org/10.1016/0016-7037(86)90178-x

Norström, E., Katrantsiotis, C., Smittenberg, R. H., & Kouli, K. (2017). Chemotaxonomy in some Mediterranean plants and implications for fossil biomarker records. In Geochimica et Cosmochimica Acta (Vol. 219, pp. 96–110). Elsevier BV. https://doi.org/10.1016/j.gca.2017.09.029

Palacas, J. G. & Lov, A. H. (1972). Hydrocarbons in Estuarine Sediments of Choctawhatchee Bay, Florida, and Their Implications for Genesis of Petroleum. In AAPG Bulletin (Vol. 56). American Association of Petroleum Geologists AAPG/Datapages. https://doi.org/10.1306/819a40ee-16c5-11d7-8645000102c1865d

Podrug, E., McClure, S.B., Kačar, S.*, Perhoč, Z., Reed, K., Tykot, R.H., Marguš, D., Mazzucco, N., Guilbeau, D., Jović, J., Ilijanić, N., Miko, S., Ivkić, I., Hajek Tadesse, V., Karp, A. In press. Krivače – results of archaeological excavation of the Middle Neolithic village and geological research of the paleolake in the Bribir-Ostrovica Valley (north Dalmatia). *Izdanja Hrvatskog arheološkog društva.*

Polissar, P. J., Uno, K. T., Phelps, S. R., Karp, A. T., Freeman, K. H., & Pensky, J. L. (2021). Hydrologic Changes Drove the Late Miocene Expansion of C4 Grasslands on the Northern Indian Subcontinent. In Paleoceanography and Paleoclimatology (Vol. 36, Issue 4). American Geophysical Union (AGU). https://doi.org/10.1029/2020pa004108

Roberts, N., Eastwood, W. J., Kuzucuoğlu, C., Fiorentino, G., & Caracuta, V. (2011). Climatic, vegetation and cultural change in the eastern Mediterranean during the mid-Holocene environmental transition. In The Holocene (Vol. 21, Issue 1, pp. 147–162). SAGE Publications. https://doi.org/10.1177/0959683610386819

Rohling, E. J., Cane, T. R., Cooke, S., Sprovieri, M., Bouloubassi, I., Emeis, K. C., Schiebel, R., Kroon, D., Jorissen, F. J., Lorre, A., & Kemp, A. E. S. (2002). African monsoon variability during the previous interglacial maximum. In Earth and Planetary Science Letters (Vol. 202, Issue 1, pp. 61–75). Elsevier BV. https://doi.org/10.1016/s0012-821x(02)00775-6

Schnurrenberger, D. (2003). In Journal of Paleolimnology (Vol. 29, Issue 2, pp. 141–154). Springer Science and Business Media LLC. https://doi.org/10.1023/a:1023270324800

Sessions, A. L. (2016). Factors controlling the deuterium contents of sedimentary hydrocarbons. In Organic Geochemistry (Vol. 96, pp. 43–64). Elsevier BV. https://doi.org/10.1016/j.orggeochem.2016.02.012

Simoneit, B. R. T. (1977). Diterpenoid compounds and other lipids in deep-sea sediments and their geochemical significance. In Geochimica et Cosmochimica Acta (Vol. 41, Issue 4, pp. 463–476). Elsevier BV. https://doi.org/10.1016/0016-7037(77)90285-x

Simonneau, A., Doyen, E., Chapron, E., Millet, L., Vannière, B., Di Giovanni, C., Bossard, N., Tachikawa, K., Bard, E., Albéric, P., Desmet, M., Roux, G., Lajeunesse, P., Berger, J. F., & Arnaud, F. (2013). Holocene land-use evolution and associated soil erosion in the French Prealps inferred from Lake Paladru sediments and archaeological evidences. In Journal of Archaeological Science (Vol. 40, Issue 4, pp. 1636–1645). Elsevier BV. https://doi.org/10.1016/j.jas.2012.12.002

Stogiannidis, E., & Laane, R. (2015). Source Characterization of Polycyclic Aromatic Hydrocarbons by Using Their Molecular Indices: An Overview of Possibilities. In Reviews of Environmental Contamination and Toxicology (pp. 49–133). Springer International Publishing. https://doi.org/10.1007/978-3-319-10638-0_2

Støren, E. N., Dahl, S. O., Nesje, A., & Paasche, Ø. (2010). Identifying the sedimentary imprint of high-frequency Holocene river floods in lake sediments: development and application of a new method. In Quaternary Science Reviews (Vol. 29, Issues 23–24, pp. 3021–3033). Elsevier BV. https://doi.org/10.1016/j.quascirev.2010.06.038

Stuiver, M., & Polach, H. A. (1977). Discussion Reporting of 14C Data. In Radiocarbon (Vol. 19, Issue 3, pp. 355–363). Cambridge University Press (CUP). https://doi.org/10.1017/s0033822200003672

Talbot, M. R. (1990). A review of the palaeohydrological interpretation of carbon and oxygen isotopic ratios in primary lacustrine carbonates. In Chemical Geology: Isotope Geoscience section (Vol. 80, Issue 4, pp. 261–279). Elsevier BV. https://doi.org/10.1016/0168-9622(90)90009-2

Vachula, R. S., Karp, A. T., Denis, E. H., Balascio, N. L., Canuel, E. A., & Huang, Y. (2022). Spatially calibrating polycyclic aromatic hydrocarbons (PAHs) as proxies of area burned by vegetation fires: Insights from comparisons of historical data and sedimentary PAH fluxes. In Palaeogeography, Palaeoclimatology, Palaeoecology (Vol. 596, p. 110995). Elsevier BV. https://doi.org/10.1016/j.palaeo.2022.110995

Velić, J., Malvić, T., Cvetković, M., & Velić, I. (2015). Stratigraphy and Petroleum Geology of the Croatian Part of the Adriatic Basin. In Journal of Petroleum Geology (Vol. 38, Issue 3, pp. 281–300). Wiley. https://doi.org/10.1111/jpg.12611

Verrecchia, E. (2007). Lacustrine and Palustrine Geochemical Sediments. In Geochemical Sediments and Landscapes (pp. 298–329). Blackwell Publishing Ltd. https://doi.org/10.1002/9780470712917.ch9

Walker, M. J. C., Berkelhammer, M., Björck, S., Cwynar, L. C., Fisher, D. A., Long, A. J., Lowe, J. J., Newnham, R. M., Rasmussen, S. O., & Weiss, H. (2012). Formal subdivision of the Holocene Series/Epoch: a Discussion Paper by a Working Group of INTIMATE (Integration of ice-core, marine and terrestrial records) and the Subcommission on Quaternary Stratigraphy (International Commission on Stratigraphy). In Journal of Quaternary Science (Vol. 27, Issue 7, pp. 649–659). Wiley. https://doi.org/10.1002/jqs.2565

Wang, H., Dong, H., Zhang, C. L., Jiang, H., Zhao, M., Liu, Z., Lai, Z., & Liu, W. (2014). Water depth affecting thaumarchaeol production in Lake Qinghai, northeastern Qinghai–Tibetan plateau: Implications for paleo lake levels and paleoclimate. In Chemical Geology (Vol. 368, pp. 76–84). Elsevier BV. https://doi.org/10.1016/j.chemgeo.2014.01.009

Wang, Y., Fang, X., Zhang, T., Li, Y., Wu, Y., He, D., & Wang, Y. (2010). Predominance of even carbon-numbered n-alkanes from lacustrine sediments in Linxia Basin, NE Tibetan Plateau: Implications for climate change. In Applied Geochemistry (Vol. 25, Issue 10, pp. 1478–1486). Elsevier BV. https://doi.org/10.1016/j.apgeochem.2010.07.002

Wang, Z., Fingas, M., Shu, Y. Y., Sigouin, L., Landriault, M., Lambert, P., Turpin, R., Campagna, P., & Mullin, J. (1999). Quantitative Characterization of PAHs in Burn Residue and Soot Samples and Differentiation of Pyrogenic PAHs from Petrogenic PAHs−The 1994 Mobile Burn Study. In Environmental Science & Technology (Vol. 33, Issue 18, pp. 3100–3109). American Chemical Society (ACS). https://doi.org/10.1021/es990031y

Weisdorf, J. L. (2005). From Foraging To Farming: Explaining The Neolithic Revolution. In Journal of Economic Surveys (Vol. 19, Issue 4, pp. 561–586). Wiley. https://doi.org/10.1111/j.0950-0804.2005.00259.x

Wiesenberg, G. L. B., Lehndorff, E., & Schwark, L. (2009). Thermal degradation of rye and maize straw: Lipid pattern changes as a function of temperature. In Organic Geochemistry (Vol. 40, Issue 2, pp. 167–174). Elsevier BV. https://doi.org/10.1016/j.orggeochem.2008.11.004

Weiss, H., & Bradley, R. S. (2001). What Drives Societal Collapse? In Science (Vol. 291, Issue 5504, pp. 609–610). American Association for the Advancement of Science (AAAS). https://doi.org/10.1126/science.1058775

Wileyto, M. (2021). Palynological Analysis of Krivače. [Unpublished undergraduate thesis]. The Pennsylvania State University.

Yu, Y., Li, Y., Guo, Z., & Zou, H. (2016). Distribution and sources of n-alkanes in surface sediments of Taihu Lake, China. In Archives of Environmental Protection (Vol. 42, Issue 1, pp. 49–55). Walter de Gruyter GmbH. https://doi.org/10.1515/aep-2016-0006

Yue, Y., Keli, Z., Liang, L., Qianhong, M., & Jianyong, L. (2019). Estimating long-term erosion and sedimentation rate on farmland using magnetic susceptibility in northeast China. In Soil and Tillage Research (Vol. 187, pp. 41–49). Elsevier BV. https://doi.org/10.1016/j.still.2018.11.011

Yunker, M. B., Macdonald, R. W., Vingarzan, R., Mitchell, R. H., Goyette, D., & Sylvestre, S. (2002). PAHs in the Fraser River basin: a critical appraisal of PAH ratios as indicators of PAH source and composition. In Organic Geochemistry (Vol. 33, Issue 4, pp. 489–515). Elsevier BV. https://doi.org/10.1016/s0146-6380(02)00002-5

Zappaterra, E. (1994). Source-Rock Distribution Model of the Periadriatic Region. In AAPG Bulletin (Vol. 78). American Association of Petroleum Geologists AAPG/Datapages. https://doi.org/10.1306/bdff90a0-1718-11d7-8645000102c1865d

Zeder, M. A. (2008). Domestication and early agriculture in the Mediterranean Basin: Origins, diffusion, and impact. In Proceedings of the National Academy of Sciences (Vol. 105, Issue 33, pp. 11597–11604). Proceedings of the National Academy of Sciences. https://doi.org/10.1073/pnas.0801317105

Zhang, X. X., Cheng, S.P., Zhu, C.J., & Sun, S.L. (2006). Microbial PAH-Degradation in Soil: Degradation Pathways and Contributing Factors. In Pedosphere (Vol. 16, Issue 5, pp. 555–565). Elsevier BV. https://doi.org/10.1016/s1002-0160(06)60088-x

Zielhofer, C., Köhler, A., Mischke, S., Benkaddour, A., Mikdad, A., & Fletcher, W. J. (2019). Western Mediterranean hydro-climatic consequences of Holocene ice-rafted debris (Bond) events. In Climate of the Past (Vol. 15, Issue 2, pp. 463–475). Copernicus GmbH. https://doi.org/10.5194/cp-15-463-2019

Zink, K.-G., Vandergoes, M. J., Mangelsdorf, K., Dieffenbacher-Krall, A. C., & Schwark, L. (2010). Application of bacterial glycerol dialkyl glycerol tetraethers (GDGTs) to develop modern and past temperature estimates from New Zealand lakes. In Organic Geochemistry (Vol. 41, Issue 9, pp. 1060–1066). Elsevier BV. https://doi.org/10.1016/j.orggeochem.2010.03.004

Appendix

1. Radiocarbon analysis

Sample ID	Fraction Modern	+/-	$\Delta^{14}C$ (‰)	^{14}C age	+/-
OSP2-195-196	0.5440	0.0019	-456.0	4890	30
OSP2-298-299	0.3141	0.0018	-685.9	9300	50
OSP2-420-425	0.3125	0.0013	-687.5	9345	35

Table 1A. Results of radiocarbon analysis for 3 selected samples. Ages are reported in calibrated years before present, or cal yrs BP.

2. Magnetic susceptibility

A magnetic susceptibility (MS) record for OSP-2 was taken after core collection at the study site. Magnetic records are a useful correlation tool to assess how local changes in the type and rate of sediment influxes. Figure 1A shows the unitless MS record from OSP-2. Transported soil and/or soils in depositional regimes are tied to higher MS values, whereas eroded soils and/or soils in erosional regimes are tied to lower MS values (Yue *et al.*, 2019). Samples between 440-300 cm demonstrate elevated MS values between 1-3 units. MS values decrease gradually between 300-200 cm to near 0 units by 200 cm. Between 200-150 cm, values increase slightly to 2 units before dropping back to 0 units by 150 cm. MS values begin to increase gradually between 150-50 cm to 1 unit before rapidly increasing between 50-0 cm to units between 3-7.

Comparison of this MS record to our current age-depth model demonstrates that the initial increase in MS between 420-300 cm is coeval with the interval of extremely high sedimentation rates (28.0 mm/yr) in the age-depth model. The lowest MS values that occur between 300-200 cm are in agreement with significantly lower sedimentation rates (0.23 mm/yr)

that then increase slightly after 200 cm (0.40 mm/yr). While the comparison of these records does not quantitatively prove the fidelity of the age-depth model and the calculated sedimentation rates, it does lend support to these values that should be further corroborated with other methods and/or at other local sites.

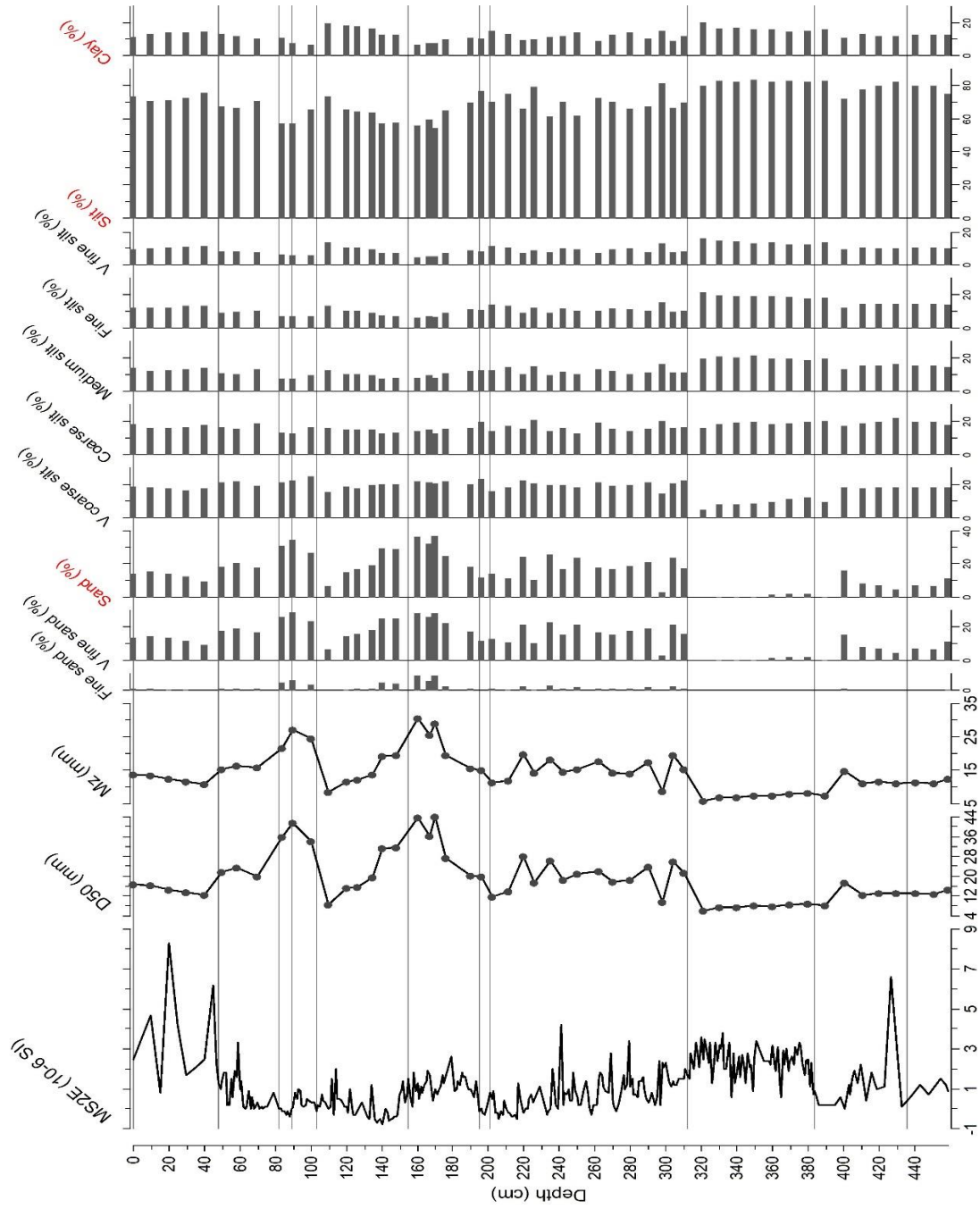

Figure 1A. From left to right, OSP-2 records of magnetic susceptibility (MS2E), 50th percentile of grain size distribution (median; D50), mean grain size (Mz), fine sand (%), very fine sand (%), sand (%), very coarse silt (%), coarse silt (%), medium silt (%), fine silt (%), very fine silt (%), silt (%), and clay (%). Records in red represent the three major categories of grain sizes. Grain classifications determined by grain diameter. The sample interval used in this investigation is outlined by red box. The dark yellow box indicates the Krivače habitation window, and the yellow shaded box indicates the window of surrounding habitation along the Dalmatia Coast.Figure modified from Nikolina Ilijanić.

4. OSP-2 pollen description

Poaceae pollen counts, divided by size, do not show significant variations through time in the study section. While high proportions of large Poaceae may have provided evidence of increased crop cultivation at Krivače, no such trends were observed. Large and small *Poaceae* appear to vary independently. Undifferentiated *Poaceae*, which included *Poaceae* grains neither diagnostically large or small, seemingly increased towards the modern, which could reflect the Middle to Late Holocene transition to warmer and more arid conditions for which grasses are better-suited. However, this is difficult to determine given the low sampling resolution.

Aquatic plant pollen counts were collected from plants including *Typha*, *Cyperaceae*, *Nymphaceae*, and *Potamogeton*. *Cyperaceae* counts are dominant at ~10% prior to the habitation interval. During the habitation interval, *Typha* counts become most abundant at ~12% while *Cyperaceae* decreases sharply to ~0%. *Cyperaceae* increases again to ~7% following the habitation interval and *Typha* counts decrease again to 0%. *Typha*, *Nymphaceae*, and *Potamogeton* counts are consistently ~0% after the habitation interval while *Cyperaceae* counts remain generally high between 10-18%. The trends in *Cyperaceae* and *Typha* across the habitation interval may reflect some change in local organic matter fluxes or nutrient cycling, but this is again difficult to determine due to the sampling resolution.

Deciduous and coniferous tree pollen reflect higher proportions of conifers before the habitation interval, reaching a peak value of ~38% at ~8100 yrs BP while deciduous pollen counts remain low near 0%. Conifer pollen counts decrease to ~0% and deciduous pollen counts increase to ~10% during the habitation interval. Following the habitation period, conifer pollen counts immediately return to high values near ~35% but exponentially decrease to 0% through the Middle Holocene while deciduous pollen counts increase from 0% to ~20% before decreasing to ~8% during the same period. Proportional shifts between deciduous and coniferous pollen

counts could help identify human land-clearing practices with additional pollen counts.

5. OSP-2 sample data

Sample #	Depth (cm)	Age (yrs BP)	% TOC	% TOC Std	Organic $\delta^{13}C$ (‰)	Organic $\delta^{13}C$ Std	$\delta^{13}C$ TIC (‰)	$\delta^{18}O$ TIC (‰)	Charcoal count (125-177um)	% $CaCO_3$
OSP-2-99-100	99.5	2863	1.7	0.1	-28.4	0	-6.26	-5.09		87.768
OSP-2-137-138	137.5	3957	4.7	0.5	-28.3	0.1	-8.36	-6.23		84.259
OSP-2-163-164	163.5	4705	0.2	0	-28.1	0.2	-8.74	-6.04		93.828
OSP-2-167-168	167.5	4820	0.3	0	-26.4	0.1				96.111
OSP-2-172-173	172.5	4964	0.4	0	-27.2	0.2	-8.55	-5.8		96.530
OSP-2-181-182	181.5	5223	0.3	0.1	-27.3	0.2	-8.15	-5.94		96.640
OSP-2-186-187	186.5	5367	0.5	0	-27.1	0.2				93.736
OSP-2-190-191	190.5	5482	0.5	0.3	-27.5	0.1	-7.32	-5.18		93.381
OSP-2-194-195	194.5	5597	1	0	-27.9	0.1	-6.39	-5.2		96.726
OSP-2-198-199	198.5	5770	0.5	0.1	-26.9	0.1	-7.21	-5.7		96.618
OSP-2-201-202	201.5	5906	1	0	-26.3	0.1	-6.75	-4.7		93.578
OSP-2-202-203	202.5	5951	0.8	0	-26.9	0.1	-6.46	-4.5		92.941
OSP-2-205-206	205.5	6087	0.7	0.3	-27.3	0.2	-6.9	-4.33		98.208
OSP-2-207-208	207.5	6178	1.1	0.1	-27.7	0				97.384
OSP-2-210-211	210.5	6315	0.4	0.2	-27.3	0.1	-5.82	-4.39		98.532

OSP-2-212-213	212.5	6405	1.5	0	-26.5	0.1	-5.68	-4	160	98.527
OSP-2-215-216	215.5	6542	0.4	0.1	-27.3	0	-5.9	-4.3		96.722
OSP-2-216-217	216.5	6587	0.3	0.1	-27	0.2	-6.26	-4.1		93.936
OSP-2-217-218	217.5	6633	0.3	0.1	-27.1	0	-5.69	-3.9	279	91.497
OSP-2-218-219	218.5	6678	0.4	0	-27.2	0.2	-5.66	-4.4		87.025
OSP-2-219-220	219.5	6723	0.6	0.1	-26.8	0.1	-5.82	-4.39		97.278
OSP-2-220-221	220.5	6769	0.6	0	-26.9	0	-5.33	-4.7		97.575
OSP-2-221-222	221.5	6814	0.8	0	-26.5	0.1	-5.89	-4.6		98.232
OSP-2-222-223	222.5	6860	0.4	0	-26.7	0.1	-5.5	-4.3	851	97.488
OSP-2-223-224	223.5	6905	0.4	0.1	-26.8	0.1	-6.24	-4.5		96.973
OSP-2-224-225	224.5	6950	0.7	0.1	-27.3	0.1	-5.55	-4.5		95.291
OSP-2-225-226	225.5	6996	1.1	0.5	-27.4	0	-5.41	-4.61	585	94.998
OSP-2-226-233	229.5	7178	1.5	0.1	-26.7	0.1	-5.84	-5.08		91.523
OSP-2-233-234	233.5	7359	1	0.1	-27.2	0.2	-6.61	-4.7		95.681
OSP-2-234-235	234.5	7405	2	0.1	-27.5	0.1	-6.52	-4.8		97.648
OSP-2-235-236	235.5	7450	1.1	0.3	-27	0.2	-6.33	-4.82		96.278
OSP-2-236-237	236.5	7495	1.2	0.1	-27.1	0.2	-6.06	-4.7		97.165
OSP-2-237-239	238	7564	1	0.4	-27.2	0	-6.13	-4.73		95.046

OSP-2-239-240	239.5	7632	1.5	0.1	-27.6	0.2	-6.53	-4.7		95.808
OSP-2-240-242	241	7700	0.9	0	-27.2	0.1	-6.77	-4.73		95.843
OSP-2-242-243	242.5	7768	1.7	0.8	-27.2	0.1	-6.84	-4.83		94.503
OSP-2-243-244	243.5	7813	0.1	0.1	-27.5	0.2	-6.42	-4.9		93.925
OSP-2-244-245	244.5	7859	0.3	0.1	-26.7	0.1	-6.23	-5.1		85.714
OSP-2-245-246	245.5	7904	2.3	0.8	-27.1	0.1	-6.1	-5.27		89.174
OSP-2-246-247	246.5	7950	0.3	0	-27.3	0.4	-5.86	-5.1		90.769
OSP-2-247-248	247.5	7995	1.8	0	-27.3	0.1	-5.85	-4.7		84.765
OSP-2-248-249	248.5	8040	1.4	0.1	-27.6	0.4	-6.26	-4.76		85.776
OSP-2-250-251	250.5	8131	0.5	0.2	-27.3	0	-6.62	-4.1		97.436
OSP-2-252-253	252.5	8222	0.2	0	-27.7	0.4	-6.97	-3.9		98.409
OSP-2-255-256	255.5	8358	0.2	0.1	-27	0.2	-6.27	-3.83	250	98.150
OSP-2-258-259	258.5	8495	0.4	0	-27.5	0.1	-0.51	-4.2		97.370
OSP-2-261-262	261.5	8631	0.5	0.2	-27.3	0.3	-5.86	-3.85		
OSP-2-263-264	263.5	8722	0.5	0	-26.6	0	-5.8	-4.32		
OSP-2-265-266	265.5	8813	0.6	0.2	-26.9	0.1	-5.88	-3.65		96.657
OSP-2-268-269	268.5	8949	0.6	0.3	-27.1	0	-6.46	-3.49		96.531
OSP-2-271-272	271.5	9085	0.4	0	-27.4	0	-5.52	-4.16		97.034

OSP-2-272-273	272.5	9131	0.5	0.2	-27.2	0	-5.21	-3.95		98.047
OSP-2-275-276	275.5	9267	0.8	0.3	-27.5	0.2	-5.37	-3.92		94.375
OSP-2-279-280	279.5	9448	1.3	0.1	-28.2	0	-3.52	-2.82		89.673
OSP-2-285-286	285.5	9721	2	0.8	-28.2	0.2	-2.58	-3.41		91.300
OSP-2-290-291	290.5	9948	1.1	0.4	-27.1	0.1	-0.94	-3.3		95.960
OSP-2-295-296	295.5	10175	1	0	-27.1	0	-0.4	-3.45		95.427
OSP-2-299-300	299.5	10311	7.3	2.5	-28	0.1	-4.41	-3.6		48.451
OSP-2-300-301	300.5	10317	3.1	1.1	-28.8	0.2	-4.47	-3.15		86.957
OSP-2-305-306	305.5	10345	0.2	0	-27.8	0.2	-4.69	-3.89		98.745
OSP-2-319-320	319.5	10425	1.3	0.4	-27.3	0.1	-2.29	-3.75		72.197
OSP-2-330-331	330.5	10488	0.4	0.1	-26.4	0	-1.71	-3.67		87.441
OSP-2-339-340	339.5	10539	0	0	-26.3	0.1	-1.68	-3.57		96.984
OSP-2-358-359	358.5	10647	0.1	0	-26.4	0.1	-0.51	-4.2		95.493

Table 2A. OSP-2 geochemical sample data.

6. Compound identification: *n*-alkanes

Target compound	SIM ions (m/z)	Retention time (RT; min)	RT window (min)
n-tridecane (C_{13})	**57,** 71, 43, 85	14.907	0.329
n-tetradecane (C_{14})	**57**, 71, 43, 85	16.828	0.201
n-pentadecane (C_{15})	**57**, 71, 43, 85	18.594	0.161
n–hexadecane (C_{16})	**57**, 71, 43, 85	20.274	0.072
n-heptadecane (C_{17})	**57**, 71, 43, 85	21.869	0.079
n-octadecane (C_{18})	**57**, 71, 43, 85	23.389	0.065
n-nonadecane (C_{19})	**57**, 71, 43, 85	24.855	0.201
n-isocane (C_{20})	**57**, 71, 43, 85	26.229	0.151
n-henisocane (C_{21})	**57**, 71, 43, 85	27.551	0.149
n-docosane (C_{22})	**57**, 71, 43, 85	28.780	0.260
n-tricosane (C_{23})	**57**, 71, 43, 85	30.048	0.173
n-tetracosane (C_{24})	**57**, 71, 43, 85	31.197	0.180
n-pentacosane (C_{25})	**57**, 71, 43, 85	32.353	0.253
n-hexacosane (C_{26})	**57**, 71, 43, 85	33.443	0.248
n-heptacosane (C_{27})	**57**, 71, 43, 85	34.454	0.179
n-octacosane (C_{28})	**57**, 71, 43, 85	35.403	0.213
n-nonacosane (C_{29})	**57**, 71, 43, 85	36.440	0.221
n-triacontane (C_{30})	**57**, 71, 43, 85	37.405	0.295
n-hentriacontane (C_{31})	**57**, 71, 43, 85	38.313	0.230
n-dotriacontane (C_{32})	**57**, 71, 43, 85	39.139	0.085
n-tritriacontane (C_{33})	**57**, 71, 43, 85	39.996	0.249
n-tetratriacontane (C_{34})	**57,** 71, 43, 85	40.868	0.246
n-pentatriacontane (C_{35})	**57**, 71, 43, 85	41.647	0.206

Table 3A. N-alkane GC-MS identification parameters including target compound name, SIM ions (m/z), retention time (RT; min), and RT window (min).

7. Compound identification: PAHs

Target compound	SIM ions (m/z)	Retention time (RT; min)	RT window (min)
Napthalene	**128**, 129, 127	5.206	0.186
Acenapthylene	**152**, 151, 153	8.267	0.179
Acenapthene	**153**, 154, 152	8.772	0.185
Fluorene	**166**, 165, 167	10.308	0.311
Phenanthrene	**178**, 176, 179	14.005	0.186
Anthracene	**178**, 179, 176	14.228	0.195
2-MP	**192**, 191, 189	16.419	0.127
9-MP	**192**, 191, 189	16.843	0.162
2,6|3,5-DMP	**206**, 205, 191	18.925	0.207
1,7-DMP	**206**, 205, 191	19.476	0.207
1,2-DMP	**206**, 205, 191	20.341	0.192
Fluoranthene	**202**, 203, 200	19.937	0.192
Pyrene	**202**, 203, 200	20.945	0.208
1,2,4-TMP	**220**	21.685?	0.153
Retene	**219**, 234	23.013	0.139
Benz[a]anthracene	**228**, 226, 229	27.728	0.232
Chrysene	**228**, 226, 229	27.875	0.235
Benzo[b]fluoranthene	**252**, 253, 250	33.427	0.162
Benzo[k]fluoranthene	**252**, 253, 250	33.572	0.196
Benzo[a]pyrene	**252**, 253, 250	34.973	0.291
Indeno[1,2,3-cd]pyrene	**276**, 277, 274	40.05	0.142
Dibenz[a,h]anthracene	**278**, 279, 276	40.556	0.168
Benzo[ghi]perylene	**276**, 277, 138	41.586	0.347

Table 4A. PAH GC-MS identification parameters including target compound name, SIM ions (m/z), retention time (RT; min), and RT window (min).

8. PAH molecules

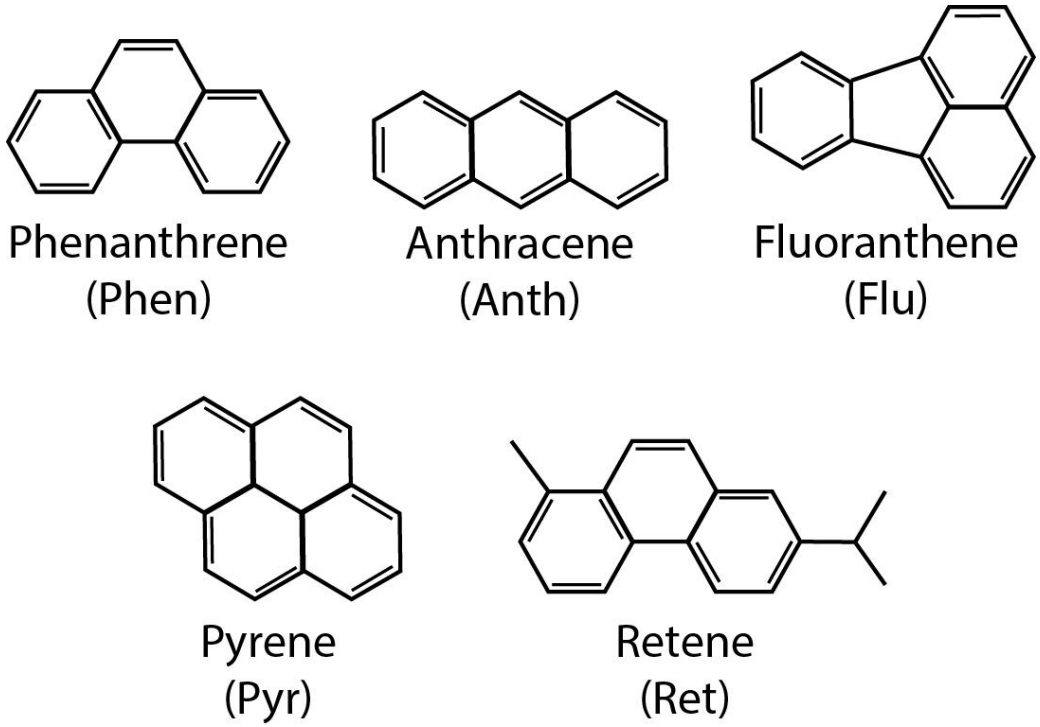

Figure 2A. Chemical structures of PAHs and their abbreviated names. Parent (pyrogenic) PAHs include phenanthrene, anthracene, fluoranthene, and pyrene. Alkylated (petrogenic) PAHs include retene.

9. Compound quantification methods

Compound classes were quantified in $ng*g^{-1}$ dry weight of sample using Equations 1a and 1b (for n-alkanes and PAHs, respectively). In these equations, RF is the response factor (ng/counts*min), which describes the amount of analyte injected versus the analyte signal captured by the GC-MS in a regression line. Here, RFs for n-alkanes and PAHs were calculated manually by extrapolating linear equations from standard-derived calibration curves. RFs determined for each compound were multiplied by A, the peak area (counts*min) of that compound. Peak area A was calculated automatically by the GC-MS program Chromeleon. The µL ratio represents the injection ratio, which is the amount of sample in the vial (µL) divided by the amount of sample injected into the GC-MS (µL). The unitless ratio represents the total amount of sample divided by the amount of sample designated for GC-MS analysis (the other

half of the sample was archived). Sample weight (g) is simply the dry weight of the sediment sample, and A indicates the area of the compound:

$$\frac{Mass\ of\ compound\ (ng)}{Mass\ of\ sample\ (g)} = \frac{\left[RF\left(\frac{ng}{area(counts \cdot min)}\right) \cdot A(counts \cdot min) \cdot \left(\frac{100\mu L}{1\mu L}\right) \cdot \left(\frac{1}{0.5}\right)\right]}{Sample\ weight\ (g)}$$

$$\frac{Mass\ of\ compound\ (ng)}{Mass\ of\ sample\ (g)} = \frac{\left[RF\left(\frac{ng}{area(counts \cdot min)}\right) \cdot A(counts \cdot min) \cdot \left(\frac{50\mu L}{1\mu L}\right) \cdot \left(\frac{1}{0.5}\right)\right]}{Sample\ weight\ (g)}$$

An example RF calculation is shown below for the n-alkane C_{29}. 5 EPA 610+ standards containing C_9 to C_{40} *n*-alkanes were run on the GC-MS to create a 5-point calibration curve. The calibration curve was forced through 0, and the amounts injected (X values) and peak areas (Y values) were recorded for each sample point on the curve. These values are recorded below in Table 1. The amounts injected and peak areas for each standard were then independently plotted in Excel and a linear equation and R^2 value were calculated. R^2 values were assessed for each compound to ensure statistical significance ($R^2 > 0.99$). The slope of the linear equation is extrapolated and used as the RF for all sample C_{29} compounds. The RF for C_{29} *n*-alkanes is 5,004,278.10 (ng/counts*min).

N-alkane calibration standard (ng/µL)	Amount injected (ng/µL)	Peak area A (counts*min)
5	9.129	45686077
10	17.98	89974533
25	39.502	197679903
50	65.478	327670132
100	87.631	438529755

Table 5A. Values recorded for C_{29} n-alkane from 5-point calibration curve.

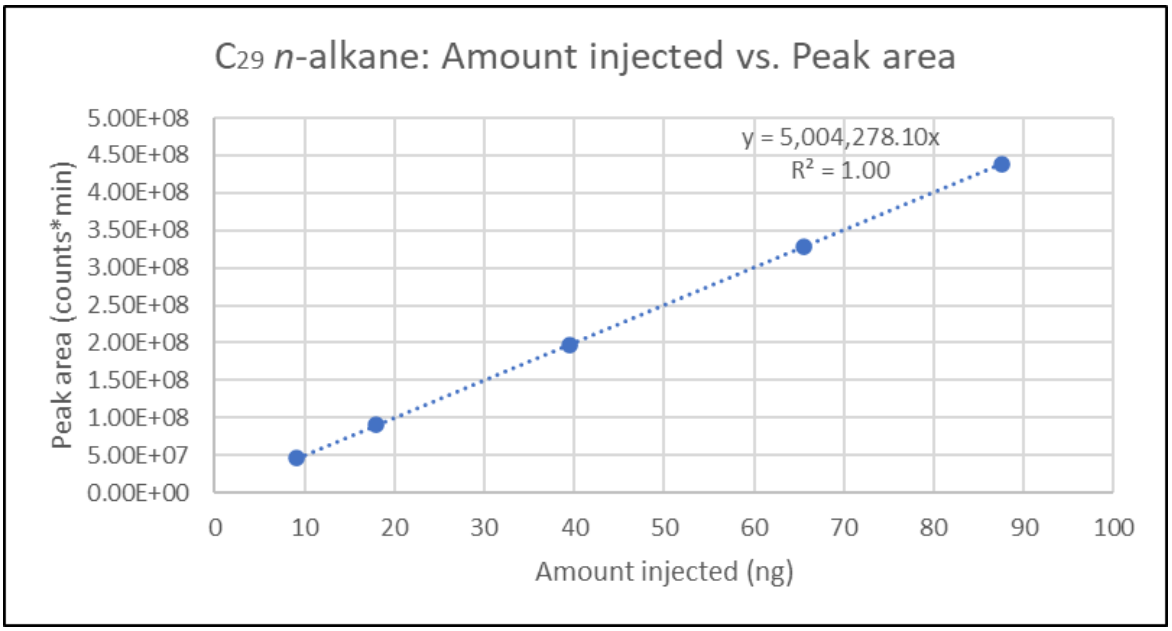

Figure 3A. Amount injected and peak area values plotted from C_{29} n-alkane values in Table 5A. Linear equation and R^2 value were extracted from the resultant plot.

An example sample quantification using the C_{29} n-alkane RF is shown below in Equation 2. For sample OSP2-136-137, the C_{29} n-alkane peak area recorded by the GC-MS was 65,244,737 counts*min. Given this information, the RF determined above, and the fist equation above, we have:

$$\frac{Mass\ of\ \ C29\ (ng)}{Mass\ of\ \ sample\ (g)} = \frac{\left[5004278.10\left(\frac{ng}{area\,(counts\cdot min)}\right)\cdot 65244737\,(counts\cdot min)\cdot\left(\frac{100\mu L}{1\mu L}\right)\cdot\left(\frac{1}{0.5}\right)\right]}{10.122\ (g)}$$

$$\frac{Mass\ of\ \ C29\ (ng)}{Mass\ of\ \ sample\ (g)} = \frac{13.038\ ng}{g}$$

For the sample OSP2-136-137, there are 13.038 ng*g^{-1} of C_{29} per dry weight of sediment sample. Note that in this equation, the units for RF–originally determined to be ng/counts*min–becomes ng/counts*min here because the denominator µL unit is accounted for in the injection ratio.

10. *N*-alkane ratios

N-alkane ratio	Description	Equation	Use
CPI_{long}	Carbon preference index of long-chain *n*-alkanes	$= \left[\left(\frac{\sum C_{27-33odd}}{\sum C_{26-33even}}\right) + \left(\frac{\sum C_{27-33odd}}{\sum C_{28-34even}}\right)\right] * 0.5$	Used to determine thermal maturity of *n*-alkanes. $CPI_{long} > 1$ = terrestrial plant contributions to sedimentary archives; $CPI_{long} < 1$ = thermally altered or mature, degraded, or more rarely, microbial/algal contributions to sedimentary archives (Bray & Evans, 1961; Freeman & Pancost, 2014; Diefendorf & Freimuth, 2017).
CPI_{short}	Carbon preference index of short-chain *n*-alkanes	$= \left[\left(\frac{C_{16} + C_{18}}{C_{15} + C_{17}}\right) + \left(\frac{C_{16} + C_{18}}{C_{17} + C_{19}}\right)\right] * 0.5$	Used to determine proportion of even vs. odd-chain *n*-alkanes, where CPI_{short} increases with thermal degradation or microbial sources and decreases with inputs from terrestrial plants (Weisenberg *et al.*, 2009).
ACL_{long}	Average chain length of odd long-chain *n*-alkanes	$= \frac{(27 * C_{27}) + (29 * C_{29}) + (31 * C_{31}) + (33 * C_{33}) + (35 * C_{35})}{C_{27} + C_{29} + C_{31} + C_{33} + C_{35}}$	Used to determine vegetation type (aquatic, macrophytic, terrestrial). $ACL_{long} \geq 31$ = C4 grasses; $ACL_{long} < 31$ = C3 woody and non-woody plants (Freeman & Pancost, 2014; Diefendorf & Freimuth, 2017).
ACL_{total}	Average chain length		Used to determine proportion of long vs.

	of all *n*-alkanes	$= \frac{(\sum z_n * n)}{\sum z_n}$	short-chain *n*-alkanes, where ACL_{total} increases with greater contributions from terrestrial plants and decreases with greater inputs from thermal degradation or microbial sources (Weisenberg *et al.*, 2009).
pAQ	Aquatic plant index	$= \frac{C_{23} + C_{25}}{C_{23} + C_{25} + C_{29} + C_{31}}$	Used to determine aquatic vs. terrestrial-sourced *n*-alkanes. Terrestrial plants = 0-0.23; macrophytes = 0.23-1 (Fiken *et al.*, 2000).

Table 6A. N-alkane ratios, ratio description, ratio equation, and the usage parameters of the ratio.

11. PAH ratios

PAH ratio	Description	Equation	Use
Retene/3-ring	Retene/retene + phenanthrene + anthracene	$= \frac{Ret}{Ret + Phen + Anth}$	Used to identify changes in the plant community burned. Retene/3-ring > 0.1 = burning of woody gymnosperms (conifers); retene/3-ring < 0.1 = burning of woody angiosperms (Simoneit, 1997; Miller *et al.*, 2017; Karp *et al.*, 2020).
APDI	Alkylated PAH derivative index	$= [f''(x) - f'(2)] \; for\ a\ parabolic\ curve$ $f(x) = ax^2 + bx + c$ $fit\ to\ a\ normalized\ distribution\ of\ alkylated\ PAHs\ (0,1,2,3\ methyl\ groups)$	Used to distinguish pyrogenic-sourced PAHs from petrogenic/coniferous-sourced PAHs. APDI > 0 (convex, decreasing) = pyrogenic; APDI < 0 (concave, increasing) = petrogenic OR conifer (Blumer & Youngblood, 1975; Laflamme & Hites, 1978; Stogiannidis & Laane, 2015; Kappenberg et al., 2019; Karp *et al.*, 2020).

Table 7A. PAH ratios, ratio description, ratio equation, and the usage parameters of the ratio.

Emma R. Hartke

M.S., Department of Geosciences, The Pennsylvania State University

Curriculum Vitae

Education

M.S. Geosciences, The Pennsylvania State University, 2022
Advisor: Katherine H. Freeman
Thesis: *Lipid biomarker records of environmental conditions and habitation during the mid-Neolithic (Dalmatia Coast, Croatia).*

B.S. Honors Geosciences, University Honors, The University of Iowa, 2020
Advisor: Bradley D. Cramer
Senior Thesis: *Decoupling $\delta^{13}C_{carb}$ and $\delta^{13}C_{org}$ at the onset of the Ireviken Carbon Isotope Excursion: $\Delta^{13}C$ and organic carbon burial (f_{org}) during a Silurian oceanic anoxic event.*

Publications

Hartke, Emma R., Cramer, Bradley D., Calner, Mikael, Melchin, Michael J., Barnett, Bruce A., Oborny, Stephan C., & Bancroft, Alyssa M., (2021). Decoupling $\delta^{13}C_{carb}$ and $\delta^{13}C_{org}$ at the onset of the Ireviken Carbon Isotope Excursion: $\Delta^{13}C$ and organic carbon burial (f_{org}) during a Silurian oceanic anoxic event. *Global and Planetary Change*, 196, 103373.

Presentations

Graduate Student Colloquium, Penn State, TALK (2022)
Hartke, Emma R., & Freeman, Katherine H. Lipid biomarker analysis (n-alkanes, PAHs) as a tool for understanding human-environmental interactions during the middle Neolithic (Dalmatia, Croatia).

Graduate Student Colloquium, Penn State, TALK (2021)
Hartke, Emma R., & Freeman, Katherine H. Lipid biomarker analysis as a tool for understanding human and environmental conditions during the middle Neolithic (Dalmatia, Croatia).

Geological Society of America National Meeting, TALK (2019)
Hartke, Emma R., Cramer, Bradley D., Calner, Mikael, Oborny, Stephan C., & Bancroft, Alyssa M. High-resolution paired organic and carbonate carbon isotope chemostratigraphy of the Ireviken Excursion (Silurian) from the Altajme core, Gotland, Sweden.

Cedar Valley Rock and Mineral Society, TALK (2019)
Hartke, Emma R., Cramer, Bradley D., Calner, Mikael, Oborny, Stephan C., & Bancroft, Alyssa M. High-resolution paired organic and carbonate carbon isotope chemostratigraphy of the Ireviken Excursion (Silurian) from the Altajme core, Gotland, Sweden.

Department Colloquium, University of Iowa, TALK (2019)
Hartke, Emma R., Cramer, Bradley D., Bandy, Terryl L., McAdams, Neo., Calner, Mikael, Oborny, Stephan C., & Bancroft, Alyssa M. Chemostratigraphy of the Silurian Ireviken Event.

NASA Iowa Space Grant Consortium, Student Research Symposium, TALK (2019)
Hartke, Emma R., Cramer, Bradley D., Calner, Mikael, Oborny, Stephan C., & Bancroft, Alyssa M. High-resolution paired organic and carbonate carbon isotope chemostratigraphy of the Ireviken Excursion (Silurian) from the Altajme core, Gotland, Sweden.

Fellowships and Awards

Krynine Scholarship, Penn State (2021)
Krynine Scholarship, Penn State (2020)
NASA Iowa Space Grant Consortium (ISGC) Fellowship, University of Iowa (2019)
Lowden Prize in Geoscience, University of Iowa (2019)
Old Gold Scholarship, University of Iowa (2016-2020)